Universidad Pública de Navarra
Nafarroako Unibertsitate Publikoa

Metamaterials for radiative cooling

Author:
Carlos Lezaun Capdevila

Supervisor:
Dr. Miguel Beruete Diaz

in the

Antenna group
Electrical, Electronics and Communication Engineering Department

June 21, 2021

Acknowledgements

First and foremost, I am sincerely grateful to Dr. Miguel Beruete for trusting me to work in an amazing research project and later accepting me as a student. Your patience to teach and guide me knows no bounds. Thank you for make me participant in fascinating researching projects and share your wisdom, it is always much appreciated.

I would like to thank to my family for their measureless love and support in my education. They have always been in the though times, for which I cannot be grateful enough. Their genuine interest in my work keeps amazing me.

I am very grateful to my friends for listening despite not understanding, far from making me feel smart, they have helped me to have a deeper knowledge of my own research and projects. Specially, thanks Rafa for showing me a world beyond the calculations, Asier for the countless geek talks and encouragement, Anel for helping me to give a helpful use of my non-engineering knowledge and Ruben, to which the distance do not mean the end of a long lasting friendship.

I am very grateful to all the researchers that have been laying the foundations that have allowed this work. Also, I must thank the Antennas Group for the good work environment and fellowship.

Thanks María José for suffering me in my madness and my apparent indifference. Our relation appears to be bulletproof because astonishingly, we are still together. I hope the following years will be easier and full of new stories.

Finally, thanks to you, the reader, for trusting this work. I hope it gives you some of the knowledge I would liked to had when I started.

PUBLIC UNIVERSITY OF NAVARRE

Abstract

Electrical, Electronics and Communication Engineering Department

Metamaterials for radiative cooling

by Carlos Lezaun Capdevila

The increasing pressure of society to decrease energy consumption and to enhance energetic efficiency has lead to search novel technologies to accomplish it. Notwithstanding the increasing electricity production of renewable energies, it is a fact that the energy expenses can be drastically reduced in most areas. Among these areas, cooling systems stand out for being energetically inefficient. Furthermore, both economical and energy cost of such systems are increasing due to the global warming, which is aggravated by the energy production for them, making a loop that is increasingly damaging the environment.

A solution to this problem has emerged under the name of radiative cooling, which is a physical phenomenon by which any terrestrial object losses heat in form of radiation that is sent to outer space. This process can be explained by black body radiation theory and the atmospheric window. The former states that any object at some temperature above 0 K radiates energy at all wavelengths, with its radiation peak and spectral location modulated by its temperature. The latter is a frequency band in which the atmosphere is transparent to radiation, making possible for waves at certain frequencies to cross freely. These phenomena allows a direct heat transmission between earth and space, which is cold and almost infinite, making a great storage for excess warmth without wasting energy in the process.

In this work, it has been studied one of the main technologies that can implement radiative cooling in practice, metamaterials, with the aim to understand how to improve its associated problems of manufacturing and design for radiative cooling applications. In Chapter 1, the fundamentals of radiative cooling are introduced along with the state of the art. Then, Chapter 2 presents the materials used in the literature and in this work to develop later analytical models for thin film multilayered metamaterials and a possible way to automatically design them. To better understand the analytical developments, two appendices introducing the underlying theory and equations are included. Also, the software used in this work is presented. Finally, the performance and analysis of three different radiative cooling devices is exposed in Chapter 3, one of them using the materials and methods of Chapter 2.

Contents

Acknowledgements iii

Abstract v

1 Introduction 1
1.1 Radiative cooling fundamentals . . . 1
1.2 Radiative cooling state of the art . . . 6

2 Materials and methods 11
2.1 Materials characterization . . . 11
2.2 Materials in this work . . . 12
2.3 Materials in the literature . . . 14
2.4 Simulators and calculators . . . 15
2.5 Mathematical models for thin film multilayered structures analysis . . . 17
2.5.1 Plane waves to transmission line analogy . . . 18
2.5.2 Concatenated transmission lines . . . 19
2.5.3 ABCD and Scattering matrix . . . 21
2.5.4 Optical method . . . 23
2.6 Evolutionary algorithms . . . 25
2.6.1 Genetic algorithm used in this work . . . 25

3 Radiative cooling designs 27
3.1 Metasurface . . . 27
3.2 Metastructure . . . 32
3.3 Multi-layered structure . . . 36

4 Conclusions and future lines 43

A Transmission line ended in a load 45

B ABCD and Scattering matrix 47

Bibliography 49

List of Figures

1.1 Black body radiation for different temperatures . . . 2
1.2 Radiative cooling principles . . . 2
1.3 Solar irradiance . . . 3
1.4 Atmospheric irradiance . . . 4
1.5 Radiative cooling coatings . . . 6
1.6 Photonic radiators examples for radiative cooling . . . 7
1.7 Manufactured thin film multilayers for radiative cooling . . . 8
1.8 Microparticle radiator . . . 8
1.9 Other radiative cooling products . . . 9

2.1 Permittivity curves in complex form of the dielectrics . . . 13
2.2 Permittivity curves in binomial form of the conductors . . . 14
2.3 CST studio picture . . . 16
2.4 GD-Calc example models . . . 17
2.5 Matlab logo . . . 17
2.6 Three concatenated transmission line model ended with a load . . . 19
2.7 Equivalent circuits of the three line model . . . 19
2.8 ABCD model for a multiple layer device . . . 22
2.9 Optic model scheme . . . 23

3.1 Metasurface . . . 27
3.2 Phosporous doped silicon permittivity . . . 28
3.3 Simulated emissivity of the reference metasurface . . . 28
3.4 Parametric sweep of the metasurface periodicity, a . . . 29
3.5 Parametric sweep of the metasurface island height, g . . . 29
3.6 Parametric sweep of the metasurface island length, l . . . 30
3.7 Parametric sweep of the metasurface island width, w . . . 30
3.8 Island distances sweep . . . 31
3.9 Angular emissivity of the metasurface . . . 31
3.10 Net cooling power over temperature of the metasurface . . . 32
3.11 Pyramidal metastructure . . . 32
3.12 Simulated emissivity of the reference metastructure . . . 33
3.13 Layer sweep with constant height . . . 34
3.14 Layer sweep with variable height . . . 34
3.15 Step sweep with 8 and 16 layers . . . 34
3.16 Comparison between GD-Calc and CST . . . 35
3.17 Angle sweep of the metastructure . . . 35
3.18 Temperature sweep of the metastructure . . . 36
3.19 Multilayered structure . . . 37
3.20 Reference radiator for the genetic algorithm . . . 38
3.21 First genetic algorithm results . . . 39
3.22 Hall of fame of the first GA . . . 39
3.23 Second genetic algorithm results . . . 40

3.24 Hall of fame of the Second GA 40
3.25 Thin film multilayered structures emissivities 41
3.26 Temperature sweep of the multilayered structures 41

A.1 Transmission line ended in a load 45
A.2 Transmission line ended in a load with an input power 45

B.1 S and ABCD matrix for a two port network 47
B.2 ABCD matrix for two connected two port network 48

Chapter 1

Introduction

Radiative cooling is a physical phenomenon by which any object emits its heat out to space in the form of radiation. This is explained by the combination of the black body radiation theory and the atmospheric window present in the earth. Such phenomenon can be used to cool buildings, devices, machinery and more, without the need of an external power supply. Therefore, it allows a new energy saving method that can be applied to different industries. Passive radiative cooling arises as an alternative to fight against global warming, which is a growing concern of the society due to its huge and potentially non reversible environmental damage. Accordingly, the topic has attracted the interest of researchers, leading to a noticeable development of the subject in recent years.

In this chapter, the main concepts behind radiative cooling are explained. Starting with the physical phenomena, it is then presented how it can be computed and measured. Then, a brief look into the state of the art serves to give an insight of how this concept is brought to reality. Finally, the way to implement a radiative cooling device using metamaterials is discussed.

1.1 Radiative cooling fundamentals

Radiative cooling is a method for transferring heat to outer space without the need of any external power supply. Such transfer is done by any object by transforming its heat into radiation. This process happens naturally under the name of black body radiation, which establishes that any object at some temperature above 0 K radiates energy at all frequencies. Such radiation increases its maximum value proportionally to the temperature of the body, being that maximum value known as peak emission. Furthermore, the wavelength of the peak emission decreases with temperature, as illustrated in Fig. 1.1.

The emissivity of an object defines both its capacity to emit and absorb energy in the form of radiation [1]. This emissivity is a function that varies with frequency and direction, in a solid angle. The solid angle is usually written as Ω and can be expressed in spherical coordinates defined by the elevation angle θ and the azimuth angle φ. In practice, the effect of azimuth angle on the emissivity can be neglected for most engineering calculations [2].

Luckily, the peak emission of the black body radiation at ambient temperature matches with the well known atmospheric transparency window. This window is a frequency band in which the atmosphere is transparent to radiation, i. e., waves at certain frequencies can cross the atmosphere and arrive to the outer space without

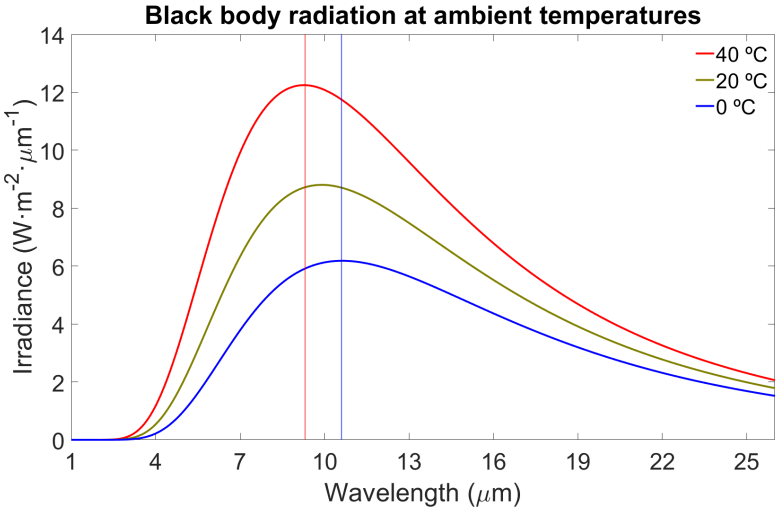

FIGURE 1.1: Black body radiation for different temperatures

being altered. It is important to note that space is at approximately 3 K and, considering its size, provides an almost infinite storage for excess heat.

The main classification for radiative cooling devices are: superambient, which considers a device at higher temperature than the environment, and subambient, for a structure at lower temperature than its surroundings. Another common classification is depending on whether it is going to operate during day or night. Those are called daytime and nighttime radiative cooling respectively.

In order to achieve a positive net cooling power and hence, a temperature reduction without any external power supply, three main elements must be considered: absorbed solar radiation (during day), atmospheric emission and the emission of the structure both in the atmospheric window and out of it [3]. For more accurate results, some authors in the literature add the thermal losses of the structure [4]. A graphical illustration of these concepts is depicted in Fig. 1.2:

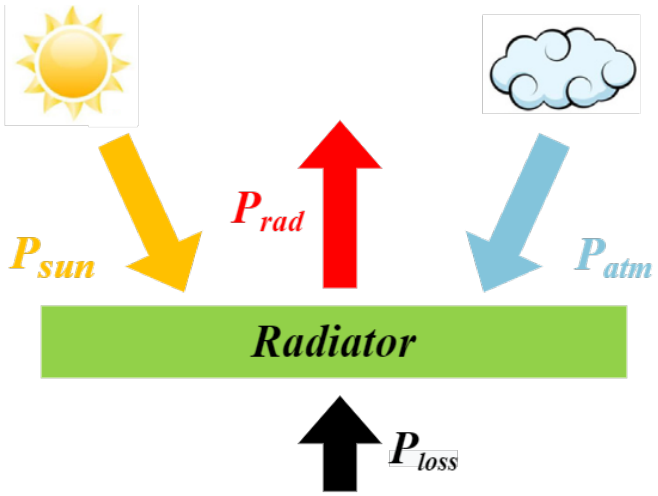

FIGURE 1.2: Radiative cooling principles [4]

Then, the net cooling power can be calculated as:

$$P_{cooling} = P_{rad} - P_{atm} - P_{sun} - P_{loss} \tag{1.1}$$

where P_{rad} is the radiated power by the structure, P_{atm} is the absorbed power from the atmosphere, P_{sun} is the captured power from the sun and P_{loss} are the thermal losses of the structure.

It can be seen in Eq. 1.1 that the radiated power by the structure is the only positive term that leads to passive cooling and the rest of terms reduce the cooling power. Therefore, it is required to reflect solar emission as much as possible and avoid absorbing the atmospheric radiation. For subambient daytime radiative cooling, more than 88% of the solar power must be reflected [5]. Such power is calculated through the sun irradiance curve, which can be extracted from [6] and has been depicted in Fig. 1.3.

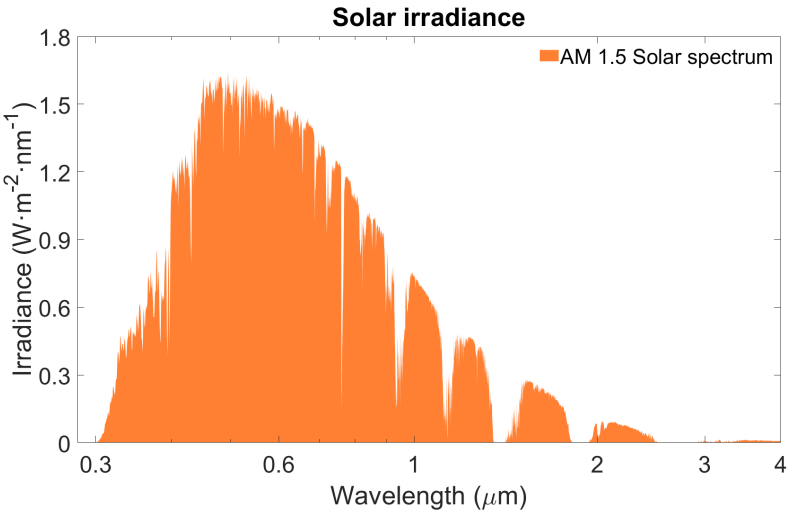

FIGURE 1.3: Solar irradiance

To calculate the power received from the sun, it is usually considered normal incidence on the structure and that the waves cross one and a half times the atmosphere. This leads to the following equation:

$$P_{sun} = A \int_0^\infty I_{AM1.5}(\lambda)\epsilon(\lambda, 0)d\lambda \tag{1.2}$$

where $\epsilon(\lambda, 0)$ is the emissivity of the cooling device in his normal direction, $I_{AM1.5}$ is the solar irradiance depicted in Fig. 1.3 and A is the area of the device, which for calculations normalized to square meters can be 1 m^2. As previously mentioned, $\epsilon(\lambda, 0)$ is a function dependent on the wavelength. It is important to note that the integral is ideally done for all wavelengths but in practice, only the band with the highest irradiance of the solar spectrum is available. Therefore, the integral is computed in the range between 0.3 μm - 4 μm.

Regarding the atmospheric absorbed power, its emissivity can be calculated from its transmittance by Eq. (1.3). Such transmittance data is obtained from [7] and used to plot the atmospheric irradiance in Fig. 1.4. This emission model considers the air

mass and the water vapour column, which is a measure of the amount of accumulated water vapour in the normal direction to the ground by the atmosphere. The atmospheric emission is usually calculated assuming that the angle dependent radiation pattern is described in a similar way as the one for a dipole radiator. This means that such pattern can be obtained knowing the maximum radiation value and respective angle, assuming an inverse cosine angular dependence with the elevation angle:

$$\epsilon_{atm} = 1 - t(\lambda)^{1/cos(\theta)} \tag{1.3}$$

where θ is the elevation angle in radians, λ the wavelength and $t(\lambda)$ the wavelength dependent irradiance spectrum of the atmosphere.

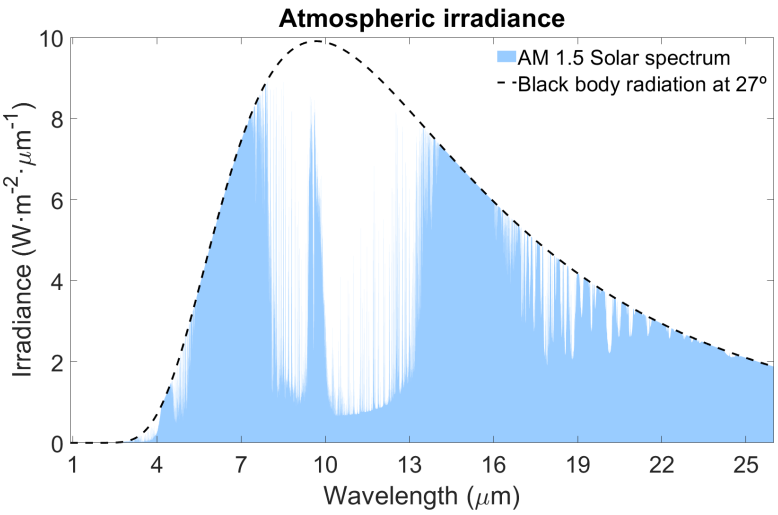

FIGURE 1.4: Atmospheric irradiance

It is important to consider that the atmosphere is not the same all over the world. Humidity, clouds, dust and weather conditions among others, limits the heat emission capacity due to its influence to the atmospheric transmittance. Therefore, there are several atmospheric transmittance curves. The absorbed atmospheric power can be calculated using the Eq. (1.4):

$$P_{atm} = A \int cos(\theta) d\Omega \int_0^{\infty} I_{bb}(T_{atm}, \lambda) \epsilon(\lambda, \theta) \epsilon_{atm}(\lambda, \theta) d\lambda \tag{1.4}$$

where $d\Omega = \int_0^{\pi/2} sin(\theta) d\theta \int_0^{2\pi} d\phi$ is the angular integral between 0-90º in elevation and 0-360º in azimut, $\epsilon(\lambda, \theta)$ is the emissivity of the structure and $\epsilon_{atm}(\lambda, \theta)$ is the atmospheric emissivity, computed as in Eq. (1.3). Recall that the two emissivities vary with both the elevation angle and the wavelength and that A is the area of the structure. I_{bb} corresponds to the black body irradiance, presented in Eq. (1.5):

$$I_{bb}(T, \lambda) = \frac{2hc^2}{\lambda^5} \frac{1}{e^{hc/\lambda k_b T} - 1} \tag{1.5}$$

where h is the Planck constant, c is the speed of light in vacuum in m/s, λ is the considered wavelength in m, k_b is the Boltzmann constant and T is the temperature of

the object in Kelvin. A few examples of the resultant temperature dependent curves are plotted in Fig. 1.1

Regarding the emissivity of the structure, it is important to consider that the atmospheric window matches the frequency band of the black body radiation at ambient temperature. Such window will set how much of the radiated power of the structure will cross the atmosphere. The emissivity of the structure can be calculated by a commercial simulator or by analytical methods. Finally, the power radiated by the structure can be obtained as:

$$P_{rad} = A \int cos(\theta) d\Omega \int_0^\infty I_{bb}(T, \lambda) \epsilon(\lambda, \theta) d\lambda \tag{1.6}$$

where all parameters have been previously defined.

In the literature, a typical concern is knowing the performance of an ideal radiator. Such device has a radiation spectra that maximizes the net cooling power and it is usually considered with a fixed emissivity. In [8] it is observed that the ideal radiator depends on both the ambient and the device temperature. This happens due to the fact that depending on both temperatures the radiated and absorbed power at a given frequency will change. That variation ends up in having more radiated power than absorbed power for some cases and vice versa. Therefore, when referring to the ideal radiator and maximum cooling power, it should be considered the expected operation temperatures. This idea also gives a better understanding of how an ideal structure should dynamically change its emission spectrum.

Another concept surrounding radiative cooling are the thermal losses. Thermal losses model the effects of the heat convection and conduction with the environment around of a cooling device. Equation (1.7) presents a typical model for computing them. For subambient radiative cooling, having thermal losses means a heat transfer from the surroundings to the structure that reduce the cooling capacity. Therefore, trying to reduce those losses as much as possible enhances the performance. For superambient radiative cooling, the opposite effect is observed. This work is aimed at cooling buildings, which means that having a device above ambient temperature, i. e. 35°, is not convenient for comfort. Hence, it is desirable to reduce thermal losses.

$$P_{loss} = hA(T_{atm} - T) \tag{1.7}$$

Where h is the heat transfer coefficient, which is usually obtained by empirical formulas. Equation (1.8) serves as an example of a possible expression to calculate this coefficient:

$$h = 2.8 + 3\mu_a \tag{1.8}$$

where μ_a is the wind speed in m/s. It is important to note that there are more complex models in the literature, where the angle of the sun, the atmospheric emissivity and the thermal losses are better fitted for a given region of the earth.

Lastly, an essential feature of a radiative cooling device is its thermal equilibrium temperature. This temperature is achieved when the radiated power equals the absorbed power by the sun, atmosphere and surroundings. In other words, it

is the stationary temperature of the device. Once defined the device emissivity and expected environmental working conditions, the equilibrium temperature can be found by numerically solving the temperature in Eq. (1.9):

$$P_{rad} = P_{atm} + P_{sun} + P_{loss} \tag{1.9}$$

where all terms have been previously defined. The temperature is usually obtained numerically due to the complexity of the expressions in the formula. Once reached this temperature, a radiative cooling device cannot achieve a lower temperature. Therefore, the thermal equilibrium temperature is desired to be below the one of the structure to be cooled in order to have an effective cooling.

1.2 Radiative cooling state of the art

In general, the materials used for radiative cooling devices are selected to fulfill two main objectives: reflect or absorb the sun radiation as much as possible, depending on the application, and emit as much energy as possible in the atmospheric window without absorbing energy out of the window. Therefore, materials can be usually classified as solar absorbent or reflective and atmospheric emissive. This leads to complex structures of multiple layers that usually are composite materials.

There are several ways to classify radiative cooling structures. In [4], a possible classification is proposed: natural radiators, coating based radiators, microparticle based radiators and photonic radiators, sometimes known as metamaterials. Also, another category for devices that do not follow the previous groups like textile coolers is included.

Coating based radiators:

These radiators are meant as a covering film for structures and, therefore, they fit well for enhancing the performance of radiative cooling structures. Such films can be made of a polymer or paint. Polymers are a widely selected option for night time radiative cooling due to its large scale production capacity and their strong emission in the atmospheric window. On the counterpart, they generally lack solar reflectance and because of its nature, they easily deteriorate over time. This goes against of the idea of a long term radiative cooler.

(a) (b)

FIGURE 1.5: Radiative cooling coatings: (a) polymer radiator [9] and (b) radiative cooling paint (TiO_2) [10]

Radiative cooling paintings present a interesting way to fit embossed surfaces. This allows to cover non smooth surfaces at the same time it keeps the production capacity for large scale applications. In general, they could be a great possibility for market application if the solar reflectance was improved. An example of both coatings is depicted in Fig. 1.5.

Photonic radiators:

Photonic radiators, also called metamaterials, are an interesting way to customize the spectral radiative properties of a structure. This is done by combining different materials, usually dielectrics and conductors, with a defined pattern. The pattern is defined by some geometry (ring, square, strip, etc.), also called meta atom, repeated along one or more axes.

Usually, two main subgroups are considered: patterned surfaces or metasurfaces, which are nearly 2D structures with a periodic geometry in its surface and multilayers o metastructures, which considers the periodic pattern in a 3D arrangement. The combination of geometries and periodization gives infinite possibilities for changing the spectral properties of a device. Some examples are shown in Fig. 1.6.

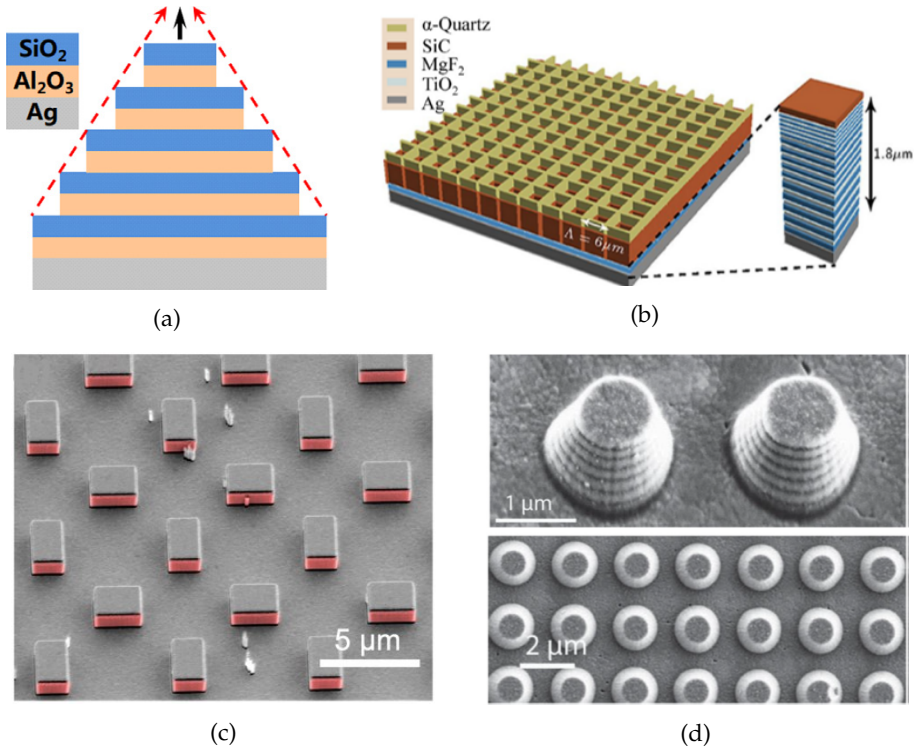

(a) (b)

(c) (d)

FIGURE 1.6: Photonic radiators examples for radiative cooling: (a) pyramid scheme from [11], (b) 3D metastructure from [12], (c) manufactured metasurface from [13] and (d) manufactured metamaterial from [14]

Although they notably surpass the other methods in terms of net cooling power, they lack large scale production methods and their design can be much harder due

to the infinite available geometries. New design techniques based on artificial intelligence are being developed in order to make such designs easier [15]. Moreover, in recent years, a new group of metamaterials has emerged under the name of thin film multilayers. Those can be though as a metamaterial with the periodization exclusively in one direction, building a 1D pattern in a 3D structure. They have the advantage of easier manufacturing methods at the cost of a slightly worse performance. Two examples are depicted in Fig. 1.7.

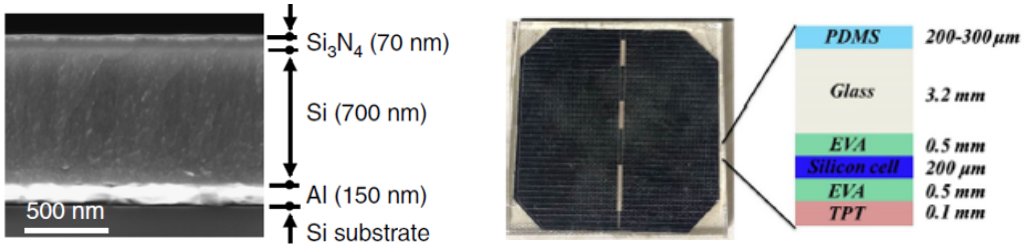

(a) (b)

FIGURE 1.7: Manufactured thin film multilayers for radiative cooling: (a) for building purposes [16] and (b) for photovoltaic cooling [17]

In order to improve the performance of thin film multilayered structures, some researchers have found doping the layers with micro spheres or micro fibers useful. Bulk materials have different optical properties to their respective microparticles. The latter can sometimes enhance the emission of the material as it happens for SiO_2. A polymer or an inorganic material can be doped with micro spheres inclusions to implement such particles. A notorious example of this approach is the one presented in [18] and depicted in Fig. 1.8.

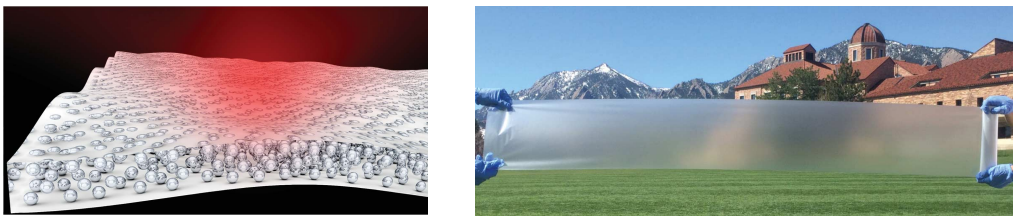

(a) (b)

FIGURE 1.8: Microparticle radiator from [18]: (a) doped polymer scheme and (b) manufactured doped polymer

Other radiators:

There are some other interesting implementations of radiative cooling. An example of a wearable cooling textile that can be of interest in hot climates is demonstrated in [19]. The textile has a metal reflector side combined with a nanoporous structure, which is similar to the micro spheres inclusion substituting the inclusion material with air, thus, leaving pores. Another material is the one found in [20], which is a near natural radiative cooler made of wood. With a process of delignification and compressing a slight net cooling power along with interesting mechanical properties for constructions is demonstrated. Both examples are shown in Fig. 1.9.

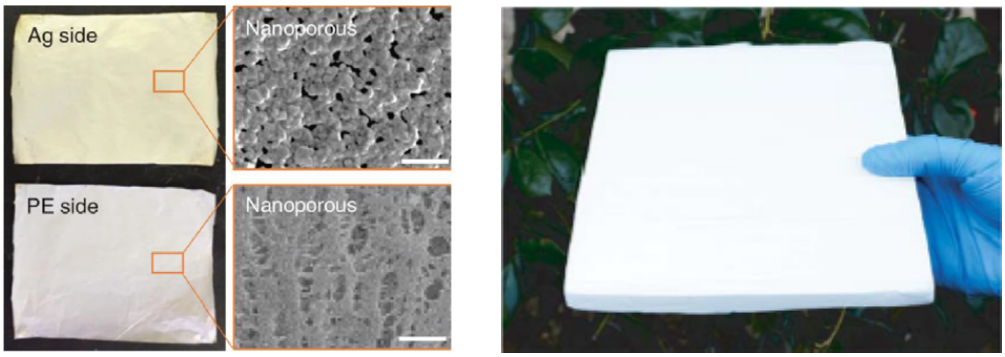

(a) (b)

FIGURE 1.9: Other radiative cooling products: (a) wearable radiative cooling fabric [19] and (b) radiative cooling wood [20]

It should be considered that, depending on the application, a thermal circuit is required to transfer the heat of an object to the radiative cooler as proposed on [21]. A good example of this are building designs where the cooling device is in the roof but the objective is not to cool the roof but the inside. For this application, water is widely used for heat transfer from the radiative cooling devices to the rooms.

Using this approach can lead to a reduction as high as 35% of energy expenses associated to building heating and cooling for the United States [20]. Such expenses are estimated to be 48% of a 430 billion dollar cost [22], leading potentially to large economic savings. Moreover, some authors see radiative cooling as a potential tool against climate change [4] because it gives the possibility to increase the natural earth heat emissions that can balance the accumulated heat by greenhouse gases. Buildings, devices, clothes, vehicles and warehouses are possible subjects to attain economic savings, comfort and enhanced durability.

Chapter 2

Materials and methods

In this chapter, the main materials employed in this work for building radiative cooling structures are presented, as well as the ones typically used in the literature. Once their properties are introduced, a brief overview of a general purpose electromagnetic simulator is presented. Then, an optical simulator based on a well known engineering software is explained. Such software is also introduced because it serves as a general computation tool that can calculate the net cooling power introduced in Chapter 1. Then, three different analytical methods that can compute the response of thin film multilayered structures are presented. Finally, a brief explanation of the genetic algorithm used for the optimization of the thin film layered structure is done.

2.1 Materials characterization

Metamaterials are usually handmade in the sense that, in general, there are no guides to select the geometries or the periodization pattern. In fact, the typical design flow is trying different configurations for a specific goal through multiple optimizations that are computationally expensive. Before selecting the geometry, it is of huge importance to select suitable materials for the final devices, in this case, radiative cooling ones.

For daytime radiative cooling, it is important that a composite meets at least one the following: large solar reflectance, large emissivity in the atmospheric window and non absorption out of the window. All these features in a material are defined by its wavelength dependent permittivity. The permittivity is a complex value that is defined in the following way:

$$\epsilon = \epsilon' - j\epsilon'' \tag{2.1}$$

where ϵ is the relative complex permittivity with ϵ' and ϵ'' as their real and imaginary parts respectively. The imaginary part is related to losses in the medium and j is the imaginary unit. For the considered wavelengths, the electromagnetic behaviour of materials is defined in literature by their complex refractive index $\tilde{n}$ through its real and imaginary parts:

$$\tilde{n} = n - jk \tag{2.2}$$

where $\tilde{n}$ is the complex refractive index, n is the real part and k the imaginary one. On one hand, n establishes the relation between the speed of light in vacuum and the phase velocity of a wave in the media. On the other hand, k is the absorption coefficient of a medium, indicating the attenuation experienced by a wave. The complex refractive index is related to the complex permittivity as:

$$\epsilon = \tilde{n}^2 = (n - jk)^2 = n^2 - k^2 + j2nk \tag{2.3}$$

where all terms has been previously defined. Taking into account Eq. 2.1, the real and imaginary parts of the permittivity can be related to the coefficients n and k:

$$\epsilon' = n^2 - k^2 \quad , \quad \epsilon'' = 2nk \tag{2.4}$$

It is also important to note that under the physics convention, the complex permittivity is defined as:

$$\epsilon = \epsilon + i\epsilon'' \tag{2.5}$$

where i is the imaginary unit in this case.

In practice, there are several mathematical models that can estimate such permittivity depending on the behaviour of the medium. Such behaviour is strongly conditioned by the electric susceptibility, χ_e, of the medium and the molecular polarizability α_T. The former is a measure of the degree of polarization of a material in response to an electric field and the later is the tendency of matter to acquire electric dipole moment when an electric field is applied.

The classical assumption of this models is that the microscopic behaviour of electrons in a solid can be treated through kinetic theory, where the displacements of the charge cloud from its central ion, or the displacement of an ion from another, produces a resonance or oscillation in the electromagnetic spectrum like a spring. One of those models that is of great interest for conductors and semiconductors in the infrared region is the Drude model. Its equation is defined as follows:

$$\epsilon = \epsilon_\infty - \frac{\omega_p^2}{j\Gamma\omega + \omega^2} \tag{2.6}$$

where ϵ is the relative permittivity, ϵ_∞ is the relative permittivity of the material when frequency tends to infinite, ω_p is the plasma angular frequency and Γ is the so called damping factor or collision frequency. Therefore, the permittivity of a material can be defined by those parameters by evaluating the formula for different values of ω, which is the angular frequency.

The damping factor Γ corresponds to the fact that when an oscillation occurs, the medium acts like a fluid that attenuates the oscillation over time. The plasma frequency γ_p is the frequency at which the real part of the permittivity of a metal becomes positive and, therefore, the metal starts to behave like a dielectric medium for the above frequencies.

2.2 Materials in this work

It is important to recall that the bandwidth of interest is between 0.3 to 26 μm and the permittivity changes over wavelength. This fact is of great interest to design selective emitters and absorbers because a material with constant permittivity cannot have a selective behaviour. Therefore, materials with little variation over the considered wavelengths are not of much interest for this application. Also, the permittivity defines the material classification as a dielectric or conductor.

A summary of all materials and their respective optical constants models used in Chapter 3 is presented in Fig. 2.1:

TABLE 2.1: Materials used in this work

Name	Form	Reference
Silicon Dioxide	SiO_2	Silicon dioxide (Glass) [23]
Amorphous Silicon	$\alpha - Si$	Silicon (amorphous) (a-Si) [23]
Silicon Nitride	Si_3N_4	Philipp 1973[24], [25]
Alumina	Al_2O_3	Querry 1985 [24]
Gold	Au	Olmon et al. 2012: single crystal[24]
Silver	Ag	Yang et al. 2015 [24]
Aluminum	Al	Rakic 1995 [24]

The complex permittivity curves of the first non metal materials in the table are depicted in Fig. 2.1 in their complex form:

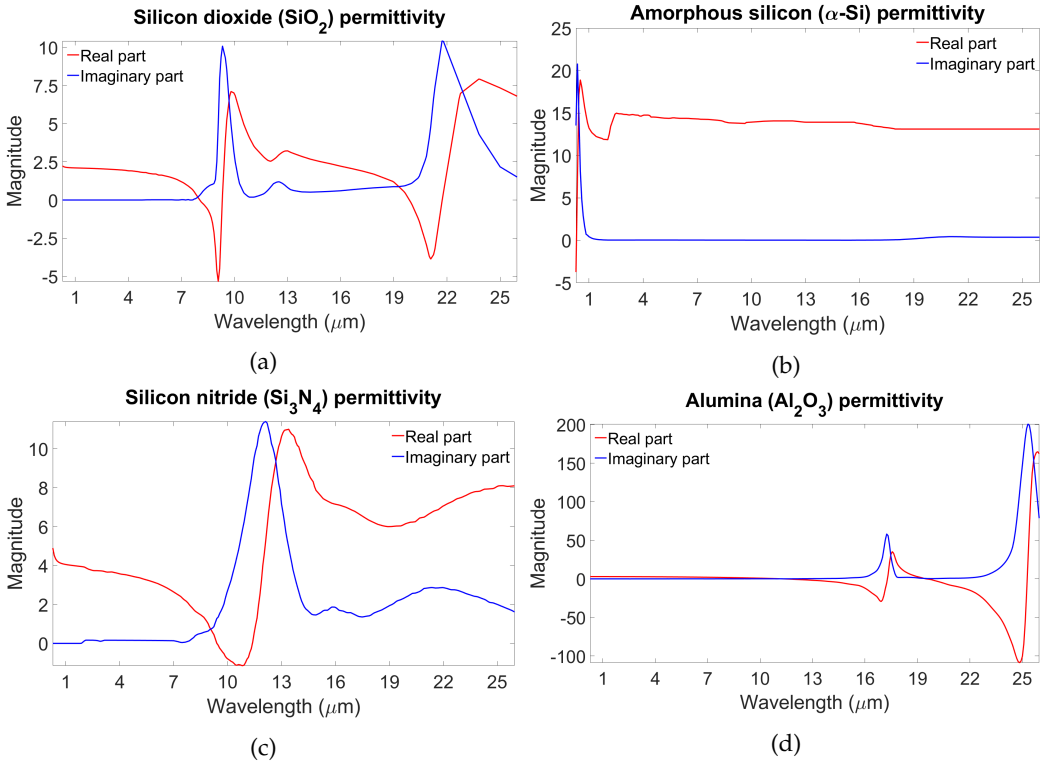

FIGURE 2.1: Permittivity curves in complex form of the dielectrics: (a) silicon dioxide, (b) amorphous silicon, (c) silicon nitride and (d) alumina

Observing the curves in Fig 2.1, it is clear that the least interesting material is the amorphous silicon because it has little variation over the considered wavelengths. This makes difficult the task of selective emission. It is important to consider that, once mixed the materials in a metastructure, the resultant permittivity is not normally a simple lineal combination of them.

Regarding the conductors, they are not as different between them as the dielectrics. This is because, by applying Eq. 2.6, the result is a negative real part and a

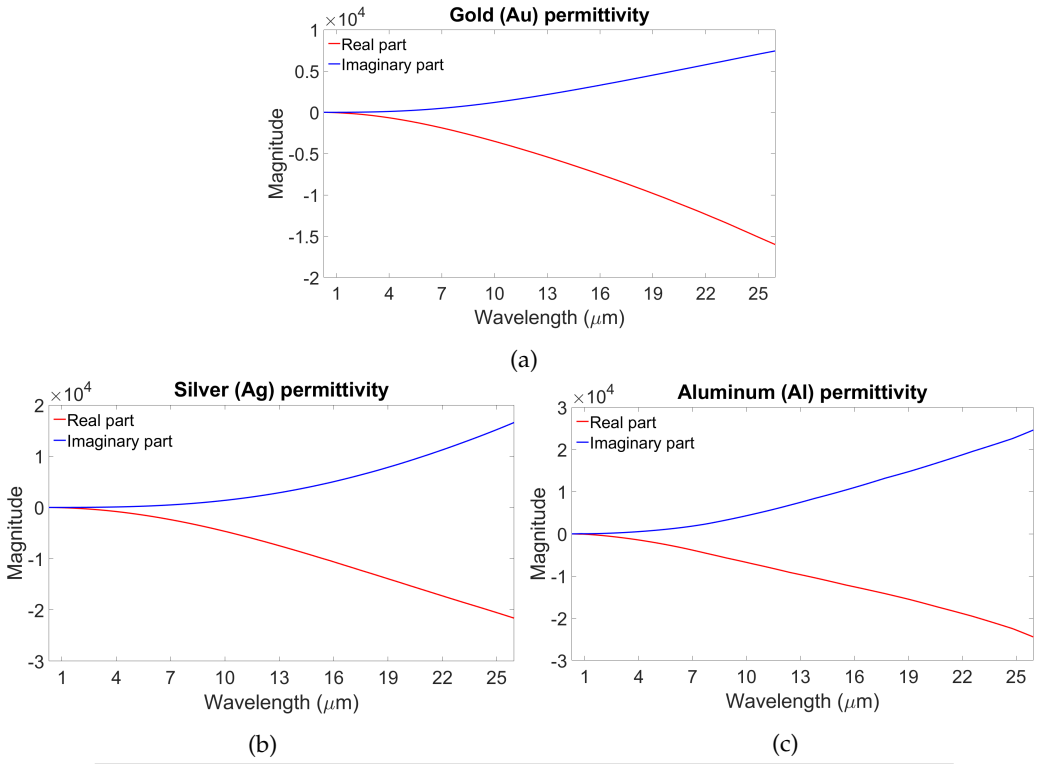

FIGURE 2.2: Permittivity curves in binomial form of the conductors: (a) gold, (b) silver and (c) aluminum

positive imaginary one without resonances for the considered wavelengths. Those curves are depicted in Fig. 2.2.

2.3 Materials in the literature

In the literature regarding radiative cooling, there are several materials typically used that are summarized in Table 2.2, which also shows the chemical formula, a classification and the use of each one. The classification is done in order to group polymers, elements and composites because they are used for different applications. Also, materials can be used for building a layer of a more complex structure, or as a substrate or reflector plane. Besides, the application of phase change materials allows to control the thermal emission. These materials are labeled as control layers. Although the materials presented in the previous section are omitted in the table, they are all used in the literature except the amorphous silicon.

Silicon is one of the most commonly used substrate. Although it is shown in the table as an element, it is usually doped with other materials such as phosphorus, like in [13]. The fluorine doped tin oxide is used with glass as a substrate in [26], but it is not commonly used though.

In general, the polymers in the table are widely used in photovoltaic applications because they are solar transmitters. This fact allows to harvest solar energy by another material at the same time the polymer radiates its heat through the atmospheric window. Therefore, they are usually in the top layer of a more complex

TABLE 2.2: Materials used in literature

Name	Form	Classification	Use	Reference
Fluorine doped tin oxide	FTO	Composite	Substrate	[26]
Silicon	Si	Element	Substrate	[13] [16]
Polymethylpentene	TPX	Polymer	Layer	[18]
Polydimethylsiloxane	$PDMS$	Polymer	Layer	[27]
Tedlar-Polyester-Tedlar	TPT	Polymer	Layer	[27]
Ethylene-vinyl acetate	EVA	Polymer	Layer	[27]
Polymethylmethacrylate	$PMMA$	Polymer	Layer	[28]
Polystyrene	PS	Polymer	Layer	[29]
aluminum doped zinc oxide	AZO	Composite	Layer	[30]
Germanium*	Ge	Element	Layer	[28] [31]
Hafnium dioxide	HfO_2	Composite	Layer	[32]
Amorphous quartz	$\alpha - SiO_2$	Composite	Layer	[12]
Silicon carbide	SiC	Composite	Layer	[12]
Magnesium fluoride	MgF_2	Composite	Layer	[12]
Titanium dioxide	TiO_2	Composite	Layer	[12] [10]
GST*	$Ge_2Sb_2Te_5$	Composite	Control layer	[33]
Vanadium dioxide	VO_2	Composite	Control layer	[34] [35]
Tungsten*	W	Element	Layer	[36]
Titanium*	Ti	Element	Reflector plane/layer	[32] [31]

*Used as a part of a thermal emitter in the infrared region, not specifically for radiative cooling.

structure.

Materials that are good thermal emitters in the infrared region should be considered in the design of radiative cooling structures. The response of those materials in the table have not been studied in the solar spectrum, but a metamaterial is usually composed of different materials, allowing the combination of solar reflective composites with thermal emitters.

Phase change materials used in radiative cooling are composites that can vary their emission spectra with temperature. This fact allows to selectively emit heat according to temperature, knowing that such temperature can come from the environment or a control system. Some research on phase change materials applied to radiative cooling has been done. Vanadium dioxide (VO_2) is a well known material with this property and is used [34] and [35] in order to have some control over thermal radiation over time. GST is another example of such composites that is used in [33]. Further research must be done in order to apply commercially these materials to radiative cooling devices.

Titanium deserves a special mention because it is a metal that is used both as a layer and a reflector plane. Titanium has low conductivity, which allows using this metal as a non reflective layer if such layer is sufficiently thin (in [31] the Ti layer has a thickness of less than 50 nm).

2.4 Simulators and calculators

CST Microwave Studio®

CST Microwave studio® is a widely used commercial simulator of the company Dassault Systèmes. This software is a powerful simulator for electromagnetic problems that provides different solvers according to them (transient, frequency domain, eigenmode...).

FIGURE 2.3: CST studio picture

The solver used in this work is the frequency domain solver, that calculates the scattering parameters of a model through the fields. These parameters are used to calculate the reflectance, transmittance and absorbance over frequency or wavelength.

The calculations are based on the *Finite Integration Technique* (FIT) and, therefore, it splits the structures into pieces (tetrahedral or hexahedral) to form a mesh in order to solve the Maxwell equations in each element. This gives information about how electromagnetic fields are distributed along the model.

Moreover, the simulator can apply periodic boundaries to a design with Floquet ports, allowing to create only the meta-atom of a metamaterial in order to know the full structure behaviour. This has the effect of speeding greatly the calculation time.

The main limitation of this software for this work is that the simulation time has an exponential relationship with the number of elements in the mesh. Besides, the mesh is generated in relation to the electric dimensions of the piece. This combined with the considered bottom wavelength (0.3 μm) ends up in a huge amount of mesh elements even being the structure of a size around hundreds of microns.

GD-Calc®

GD-Calc® stands for *Grating Diffraction Calculator* and is a Matlab® based software developed by Ken Johnson. This software is sometimes used in optics due to its performance and reduced computation time compared to more general simulators. The simulator can be downloaded through the codeocean platform [37] with the documentation and is introduced in the webpage [38].

This software is based on the semi analytic method called *Rigorous Coupled Wave Method* (RCWM) to compute the diffraction efficiencies. Therefore, its computation time does not depend on the electrical size of the structure like in CST, allowing to simulate electrically large structures in the terahertz and optical range. Through the diffraction efficiencies, the reflectance and transmittance can be obtained, and from

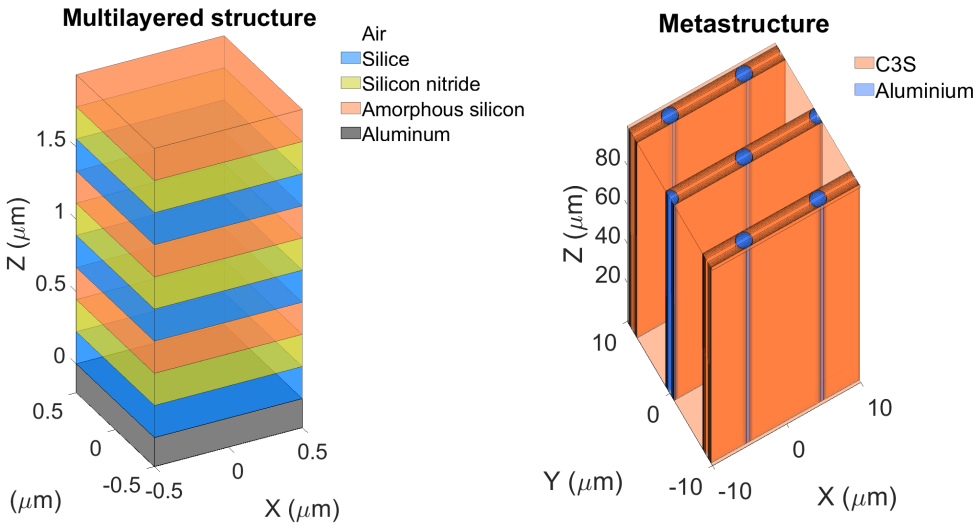

FIGURE 2.4: GD-Calc example models: (a) thin film multilayer and (b) metastructure

them, the absorption and emissivity of a model.

Matlab®

Matlab® is a well known engineering software that is widely used for a large variety of scientific fields. It has its own programming language and includes a lot of built-in functions and packages that facilitates the program design. This software has been used to calculate the net cooling power equations presented in Chapter 1 and to develop the analytic methods for multilayered thin film structures developed at the end of this chapter. Besides, it has the advantage of being designed to make vector and matrix calculus easy.

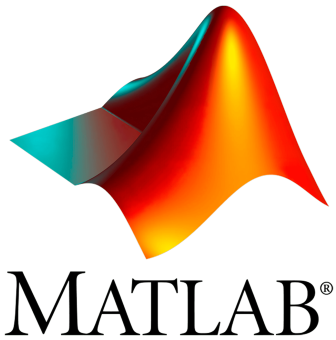

FIGURE 2.5: Matlab logo

2.5 Mathematical models for thin film multilayered structures analysis

Thin film multilayered structures are a specific case of metamaterials in which the pattern is exclusively in one direction. This makes the analytical methods much

easier to develop than for patterns in two or more directions. Therefore, time consuming simulations can be replaced by equations and matrix calculations, which can obtain the emissivity of a structure much faster.

In this section, different analytical methods for calculating the reflectance and transmittance of a thin film structure are developed and presented. The first two are based on transmission line theory, which can have a similar behaviour as a multilayered structure, as explained in the next subsection. The third method is the one presented in [39], and is based on plane wave propagation theory.

2.5.1 Plane waves to transmission line analogy

It is well known from [40] that a complete analogy between a propagating plane wave in a medium and a wave flowing through a transmission line can be done. This analogy allows to identify the intrinsic characteristics of a plane wave with the voltage wave, current wave and the propagation constant γ of a transmission line using the impedance concept.

$$E_x(z) = E_+e^{-jkz} + E_-e^{jkz} \quad (2.7) \qquad V(z) = V_+e^{-\gamma z} + V_-e^{\gamma z} \quad (2.8)$$

$$H_y(z) = \frac{1}{\eta}[E_+e^{-jkz} - E_-e^{jkz}] \quad (2.9) \qquad I(z) = \frac{1}{Z_0}[V_+e^{-\gamma z} - V_-e^{\gamma z}] \quad (2.10)$$

On the left side, $E_x(z)$ and $H_y(z)$ are the electrical and magnetic field vectors of a plane wave travelling in the z direction. The subscripts x and y refer to the direction of the vectors and the subscripts $+$ and $-$ are the progressive and regressive waves respectively, k is the wave number and η is the intrinsic impedance of a medium.

On the right side, $V(z)$ and $I(z)$ are the voltage and current wave flowing through a transmission line in one direction, that is considered z, γ is the propagation constant of the line and Z_0 its characteristic impedance.

The wave vector k and the propagation constant γ are defined as follows:

$$k = \frac{\omega}{C_0}\sqrt{(\mu_r' - j\mu_r'')(\epsilon_r' - j\epsilon_r'')} \quad (2.11) \qquad \gamma = \sqrt{(R + j\omega L)(G + j\omega C)} \quad (2.12)$$

where ω is the angular frequency, μ_0 the magnetic permeability of vacuum and C_0 the speed of light in vacuum, and μ_r is the relative magnetic permeability with their real and imaginary parts μ_r' and μ_r''. Such relative permeability is usually assumed equal to 1, that is to say, the same as the one of vacuum. ϵ_r is the relative complex permittivity of a medium, as defined in Eq. 2.4 and ϵ_0 the permittivity of the vacuum. R and L are the real and imaginary parts of a generic impedance Z, G and C are the respective real and imaginary parts of a complex capacitance C. Both R and C are factors of a transmission line normalized to its unit length. k and γ are respectively the wave vector and the propagation constant of a medium and a transmission line.

The intrinsic impedance η and the characteristic impedance Z_0 are:

$$\eta = \eta_0\sqrt{\frac{\mu_r' - j\mu_r''}{\epsilon_r' - j\epsilon_r''}} \quad (2.13) \qquad Z_0 = \sqrt{\frac{R + j\omega L}{G + j\omega C}} \quad (2.14)$$

where η_0 is the intrinsic impedance of vacuum, calculated as $\eta_0 = \sqrt{\mu_0/\epsilon_0}$ and the rest of the terms have been previously defined. Then, a transmission line can match the electromagnetic response of a medium in all details and, therefore, the response of a medium can be analyzed by its equivalent transmission line. For such calculations, the presented equations for a plane wave (left side equations) can be substituted for their equivalent transmission line formulas (right side equations). It should be noted that this notation hinders the analogy by considering every parameter as a complex number. The analogy is better understood in the easier case when real numbers are considered.

2.5.2 Concatenated transmission lines

An example of three concatenated transmission lines terminated in a load is depicted in Fig. 2.6. This model is equivalent to three different dielectric layers and thicknesses between two media with characteristic impedances η_0 and η_L respectively. Such equivalence has been introduced in the previous subsection.

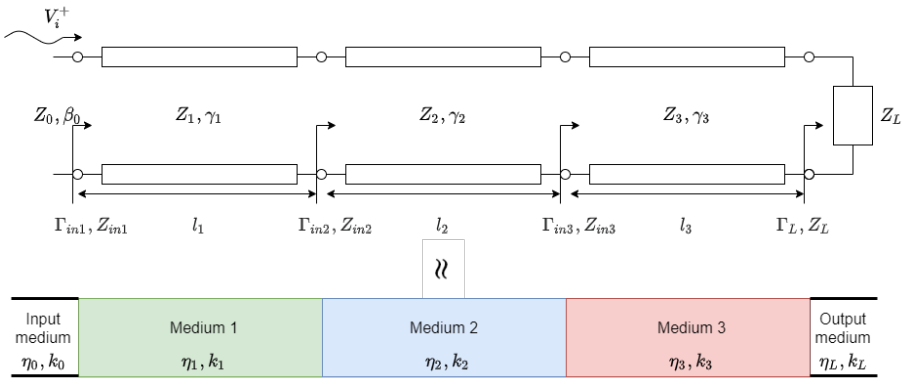

FIGURE 2.6: Three concatenated transmission line model ended with a load

Where V_i^+ is the progressive input voltage wave, Z_n and γ_n are the impedance and propagation constant of the equivalent transmission line of the respective medium, l_n its length, β_0 is propagation constant of the input medium (air). $Z_{in(n)}$ and $\Gamma_{in(n)}$ are the input impedance and reflection coefficient of each equivalent transmission line. η_n and k_n are respectively the characteristic impedance and wave number of a medium that can be matched with Z_n and γ_n.

The following equivalent circuits are used to obtain the reflectance and transmittance of the whole circuit by splitting the problem.

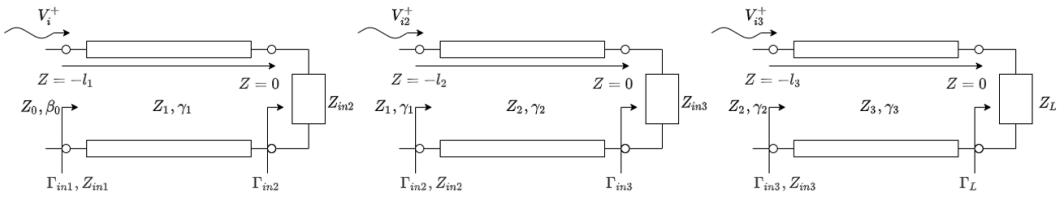

FIGURE 2.7: Equivalent circuits of the three line model

Where $P_{L(n)}$ is the power delivered to the equivalent input impedance of each section. Beginning in the load and applying the equations A.2 and A.1, the input impedance and reflection coefficient of each section are calculated as:

$$Z_{in(2)} = Z_2 \frac{Z_{in(3)} + Z_2 tanh(\gamma_2 l_2)}{Z_2 + Z_{in(3)} tanh(\gamma_2 l_2)} \qquad Z_{in(1)} = Z_1 \frac{Z_{in(2)} + Z_1 tanh(\gamma_1 l_1)}{Z_1 + Z_{in(2)} tanh(\gamma_1 l_1)} \tag{2.15}$$

$$\Gamma_3 = \frac{Z_{in(3)} - Z_2}{Z_{in(3)} + Z_2} \qquad \Gamma_2 = \frac{Z_{in(2)} - Z_1}{Z_{in(2)} + Z_1} \qquad \Gamma_1 = \frac{Z_{in(1)} - Z_0}{Z_{in(1)} + Z_0} \tag{2.16}$$

where $Z_{in(3)}$ has been omitted since it is similar to equation A.2. Both equations, can be generalized in a recursive calculation in the following way:

$$Z_{in(n)} = Z_n \frac{Z_{in(n+1)} + Z_n tanh(\gamma_n l_n)}{Z_n + Z_{in(n+1)} tanh(\gamma_n l_n)} \tag{2.17}$$

$$\Gamma_{in(n)} = \frac{Z_{in(n)} - Z_{(n-1)}}{Z_{in(n)} + Z_{(n-1)}} \tag{2.18}$$

It is important to consider that in the previous equations, the load impedance would be the fourth one: $Z_L = Z_4$ and $\Gamma_L = \Gamma_4$.

Once the impedances and the reflection coefficients are known, the power transmitted can be calculated in a similar way. The power delivered to the second transmission line is omitted because is similar to the model of a loaded transmission line. Following equation A.5 in the equivalent circuits of figure 2.7, the power delivered to each transmission line is:

$$P_{L3} = P_{L2} e^{-2\alpha_2 l_2} \frac{1 - |\Gamma_{in3}|^2}{1 - |\Gamma_{in3}|^2 e^{-4\alpha_2 l_2}} \qquad P_L = P_{L3} e^{-2\alpha_3 l_3} \frac{1 - |\Gamma_L|^2}{1 - |\Gamma_L|^2 e^{-4\alpha_3 l_3}} \tag{2.19}$$

where α_n is the real part of the propagation constant γ_n of each medium and the rest of the terms have been previously defined. If the load is considered as the fourth element $P_L = P_{L4}$, then, the following expression can be used:

$$P_{Ln} = P_{L(n-1)} e^{-2\alpha_{(n-1)} l_{(n-1)}} \frac{1 - |\Gamma_{in(n)}|^2}{1 - |\Gamma_{in(n)}|^2 e^{-4\alpha_{(n-1)} l_{(n-1)}}}, \qquad n > 1 \tag{2.20}$$

Which for computing the transmission coefficient must be divided by the input power, as presented in Appendix A:

$$T_n = \frac{P_{Ln}}{P_g} \tag{2.21}$$

where T_n is the transmission coefficient to each medium, P_{Ln} is the power delivered to each equivalent impedance and P_g is the power at the input, established by V_i^+ and the input impedance Z_{in1}.

Knowing the electromagnetic characteristics and the thicknesses of the materials, both the reflection and transmission coefficient of each medium can be calculated analytically. Thus, there is no need to use a simulator for calculating the reflectance of a thin film multi layer with n layers of different material and thickness. Considering an incident wave as in Fig. 2.6 and taking into account the analogy between a transmission line and a plane wave and the transmission line solution of Appendix

A, the reflectance and transmittance in the first port of a structure can be obtained through its transmission and reflection coefficients as:

$$R = |\Gamma_{in1}|^2 \tag{2.22}$$

$$T = |T_L|^2 \tag{2.23}$$

where R is the reflectance and T the transmittance.

2.5.3 ABCD and Scattering matrix

The fact that a multilayered structure can be modeled as multiple transmission lines, allows to use other analytical methods which are equivalent to the previous one. A two port network can be defined by different matrix definitions and, for this work, the ABCD and scattering matrix definitions are used. The formulation around these matrix are introduced in Appendix B.

The elements of the ABCD matrix can be calculated by applying its definition, which is introduced in [40]. Adding the voltage and current wave formulas presented in Eq. 2.8 and 2.10 and expanding the matrix operation of equation B.5, the transmission coefficients of a lossy transmission line can be obtained as:

$$A = \frac{V_1}{V_2}|_{I_2=0} = \frac{V_0^+(e^{\gamma l} + \Gamma e^{-\gamma l})}{V_0^+(e^0 + \Gamma e^0)} = \frac{e^{\gamma l} + e^{-\gamma l}}{2} = cosh(\gamma l) \tag{2.24}$$

$$B = \frac{V_1}{I_2}|_{V_2=0} = \frac{V_0^+(e^{\gamma l} + \Gamma e^{-\gamma l})}{\frac{V_0^+}{Z_0}(e^0 - \Gamma e^0)} = \frac{Z_0(e^{\gamma l} - e^{-\gamma l})}{2} = Z_0 sinh(\gamma l) \tag{2.25}$$

$$C = \frac{I_1}{V_2}|_{I_2=0} = \frac{\frac{V_0^+}{Z_0}(e^{\gamma l} - \Gamma e^{-\gamma l})}{V_0^+(e^0 + \Gamma e^0)} = \frac{e^{\gamma l} - e^{-\gamma l}}{2Z_0} = \frac{sinh(\gamma l)}{Z_0} \tag{2.26}$$

$$D = \frac{I_1}{I_2}|_{V_2=0} = \frac{\frac{V_0^+}{Z_0}(e^{\gamma l} - \Gamma e^{-\gamma l})}{\frac{V_0^+}{Z_0}(e^0 - \Gamma e^0)} = \frac{e^{\gamma l} + e^{-\gamma l}}{2} = cosh(\gamma l) \tag{2.27}$$

with γ as the complex wave number of the medium, Z_0 the characteristic impedance of the equivalent transmission line and l its length. V_p and I_p refer to the voltage and current at the input of the respective port of the system and V_0^+ is the progressive voltage wave in a transmission line. It is important to note that in the equations, $I_2 = 0$ indicates an open circuit at the end of the transmission line ($\Gamma = 1$) and $V_2 = 0$ a short circuit ($\Gamma = -1$). Also, for convenience the position at the beginning (port 1) is chosen as $Z = -l$ and at the end is $Z = 0$ (port 2). Therefore, equation B.5 can be rewritten for a lossy transmission line as:

$$\begin{bmatrix} V_1 \\ I_1 \end{bmatrix} = \begin{bmatrix} cosh(\gamma l) & Z_0 sinh(\gamma l) \\ sinh(\gamma l)/Z_0 & cosh(\gamma l) \end{bmatrix} \begin{bmatrix} V_2 \\ I_2 \end{bmatrix} \tag{2.28}$$

A series of n lossy transmission lines represented by their respective ABCD matrix will be equivalent to a multilayered structure. Such model is graphically represented in Fig. 2.8:

Following equation B.6 and excluding the input and output medium, the model will satisfy the formula:

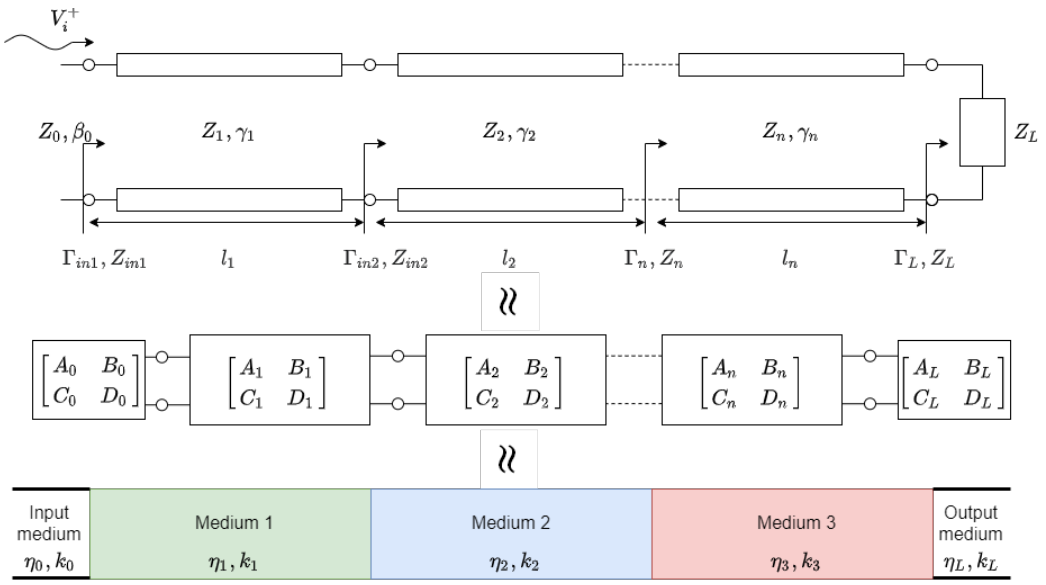

FIGURE 2.8: ABCD model for a multiple layer device

$$\begin{bmatrix} V_1 \\ I_1 \end{bmatrix} = \begin{bmatrix} cosh(\gamma_1 l_1) & Z_1 sinh(\gamma_1 l_1) \\ sinh(\gamma_1 l_1)/Z_1 & cosh(\gamma_1 l_1) \end{bmatrix} \begin{bmatrix} cosh(\gamma_2 l_2) & Z_2 sinh(\gamma_2 l_2) \\ sinh(\gamma_2 l_2)/Z_2 & cosh(\gamma_2 l_2) \end{bmatrix} \cdots \\ \cdots \begin{bmatrix} cosh(\gamma_n l_n) & Z_n sinh(\gamma_n l_n) \\ sinh(\gamma_n l_n)/Z_n & cosh(\gamma_n l_n) \end{bmatrix} \begin{bmatrix} V_n \\ I_n \end{bmatrix} \tag{2.29}$$

This procedure computes the total equivalent ABCD matrix of all the transmission lines, which can match its electromagnetic response with a multi layer structure. Once the transmission coefficients have been calculated, Eq. B.7-B.10 will add the input and output medium at the same time as it makes the calculations of the scattering parameters. Through the scattering parameters, the transmittance and reflectance can be obtained:

$$R_1 = |S_{11}|^2 \qquad R_2 = |S_{22}|^2 \tag{2.30}$$

$$T_1 = |S_{21}|^2 \qquad T_2 = |S_{12}|^2 \tag{2.31}$$

where R_p and T_p are respectively the reflectance and the transmittance seen in a port of the system, S_{ij} are the scattering parameters that are related to the transmission matrix as presented in Appendix B.

It should be considered that the models of the previous subsections had considered normal incidence over the structure. That is the reason why there has not been any angular dependency in the introduced equations, but in practice, the emissivity of a structure must be defined for all incident angles. The generalization of the previous models for oblique angle incidence is explained in [40]. First, the propagation angle in each medium can be known by applying the Snell law:

$$\theta_n = asin\left(\frac{\gamma_0}{\gamma_n} sin\theta_0\right) \tag{2.32}$$

where θ_n is the propagation angle of the wave in the medium n, θ_0 and γ_0 are the incident angle and propagation constant in the incident medium and γ_n is the phase constant in the medium n. Once the angles in each medium are defined, the propagation constant γ is redefined as:

$$\gamma'_n = \gamma_n cos(\theta_n) \tag{2.33}$$

where γ'_n is the propagation constant in a medium that takes into account a non normal propagation direction. Finally, the impedances depend on the incident angle and the propagation mode states such dependency in the following way:

$$Z'_{TM(n)} = Z_n cos(\theta_i) \qquad for\ TM\ polarization \tag{2.34}$$

$$Z'_{TE(n)} = Z_n sec(\theta_i) \qquad for\ TE\ polarization \tag{2.35}$$

where $Z'_{TM(n)}$ and $Z'_{TE(n)}$ are the impedance in the medium n experienced by a TM wave and a TE wave respectively. This new phase constants and impedances must be replaced in Eq. 2.16, Eq. 2.19 and Eq. 2.29 in order to generalize the electromagnetic response to oblique incident angles.

2.5.4 Optical method

A mathematical method for analysing multilayered structures is presented in [39]. In this case, plane wave propagation theory is used to compute the electromagnetic response of the system. Consider the illustration of Fig. 2.9.

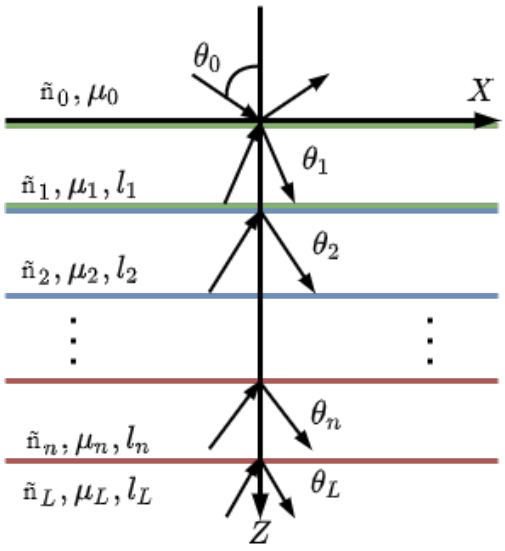

FIGURE 2.9: Optic model scheme

Regarding Fig. 2.9, $\tilde{n}_n$, μ_n and l_n are the refractive index as presented in Eq. 2.2, the relative permittivity of Eq. 2.1 and the thickness of the layer respectively. In this method, the incident angle θ_0 is considered from the beginning. Such angle in each medium can be obtained from the following expression:

$$\theta_n = acos\left(\sqrt{1 - \left(\frac{\tilde{n}_0 sin(\theta_0)}{\tilde{n}_n}\right)^2}\right) \tag{2.36}$$

where θ_n is the propagation angle in the medium n, and θ_0 and $\tilde{n}_0$ are the incident angle and the complex refractive index of the first medium. This equation can be derived by applying the law of Snell combined with the well known trigonometric identity: $cos^2(x) + sin^2(x) = 1$. The propagation constant is redefined again in the following way:

$$a_n = \frac{\gamma'_n}{\gamma_n} \quad , \quad b_n = \frac{\tilde{n}_n}{\mu_n} \quad , \quad g_n = a_n b_n \tag{2.37}$$

where g_n is the redefined propagation constant, γ_n and γ'_n have been defined in Eq. 2.12 and Eq. 2.33, $\tilde{n}$ is the complex refractive index of 2.2 and μ_n is the relative magnetic permeability that it is usually assumed as 1. Then, the transmission matrix can be defined as:

$$\begin{bmatrix} A_n \\ B_n \end{bmatrix} = P_n D_n^{-1} D_{n+1} \begin{bmatrix} A_{n+1} \\ B_{n+1} \end{bmatrix} \tag{2.38}$$

where P_n is the propagation matrix:

$$P_n = \begin{bmatrix} e^{-\gamma'_n l_n} & 0 \\ 0 & e^{\gamma'_n l_n} \end{bmatrix} \tag{2.39}$$

and D_n is the transfer matrix, which depends on the polarization of the incident wave:

$$D_{TE(n)} = \begin{bmatrix} 1 & 1 \\ g_n & -g_n \end{bmatrix} \qquad for\ TE\ polarization \tag{2.40}$$

$$D_{TE(n)} = \begin{bmatrix} a_n & a_n \\ b_n & -b_n \end{bmatrix} \qquad for\ TM\ polarization \tag{2.41}$$

where all terms have been previously defined. In order to compute the total transfer matrix, the contribution of every layer must be multiplied by the rest of them. This leads to the following formula:

$$\begin{bmatrix} A_1 \\ B_1 \end{bmatrix} = M \begin{bmatrix} A_n \\ B_n \end{bmatrix}, \ where \ \ M = \prod_{n=1}^{N-1} P_n D_n^{-1} D_{n+1} = \begin{bmatrix} M_{1,1} & M_{1,2} \\ M_{2,1} & M_{2,2} \end{bmatrix} \tag{2.42}$$

where Mij terms are the transmission coefficients of the total transfer matrix M and N is the number of layers. If we assume that there is only an incident wave at the input ($B_1 = 0$) and the result is normalized to such input ($A_1 = 1$), then, the transmission and reflection coefficients are:

$$t = \frac{1}{M_{1,1}} \quad , \quad r = \frac{M_{2,1}}{M_{1,1}} \tag{2.43}$$

Finally, the transmittance and reflectance can be computed using the previous coefficients:

$$T = \frac{Re(\tilde{n}_N)}{Re(\tilde{n}_1)} \frac{Re(cos\theta_N)}{Re(cos\theta_1)} tt^* \quad , \quad R = rr^* \tag{2.44}$$

where *Re* denotes the real part of a number, the superscript * the complex conjugate of a number and $_N$ the last layer.

2.6 Evolutionary algorithms

Evolutionary algorithms are searching and optimization methods that are a subgroup of artificial intelligence and are based on the postulates of biological evolution. A solution to a problem is called an individual, and a set of entities that constitute several solutions are named as population. An individual is defined by its chromosome, which is a code that can identify it. Each number of this code is called a gene. Once given a population, the individuals can experience the following genetic operators:

1. Reproduction: That is when two individuals cross their chromosomes to give a new individual. This allows to follow a certain direction in the search of a solution.

2. Mutation: That is the process of randomly changing the chromosome of one individual in order to increase the chance of finding a whole different solution.

3. Recombination or crossover: This is the combination of the chromosome of two or more individuals that can differ from the solutions found by the parents. It allows a wider search of the solution.

4. Selection: This is the process of discarding some of the resultant individuals of the previous operations in order to have a certain population size in the next generation.

Regarding more general characteristics of optimization algorithms, the sample space or search space is the number of possible individuals, or solutions to a problem, and is defined by the size of the chromosome. It is very common to put some restrictions to the problem in order to reduce such space or to omit solutions that cannot be put into practice. Also, an error function must be defined to measure the suitability of the individuals for a given solution. Such function is a mathematical operation that measures the suitability of a given solution with the desired solution and is usually called fitness function. Combining this function with the genetic operators, a search for the ideal solution through evolution can occur.

2.6.1 Genetic algorithm used in this work

The genetic algorithm is one of the options developed in the evolutionary algorithms field and it is inspired by the process of natural selection. It usually starts with a randomly created initial population that will give the next generation through the genetic operators described previously. This process will be repeated until one of the stop conditions are met, which are time limit, maximum number of generations or maximum number of generations without improvement in the fitness function. By its philosophy, this algorithms is not going to know when it has found the best possible solution if this case is met, and it is going to keep searching until one of the conditions is met.

Following the biological analogy, the population size or generation size is the number of individuals in each generation. A generation is a set of individuals and

the best solution among them, the best individual, is usually called hall of fame. This best individual will have the minimum value for the fitness function among a generation. With the operations of the list and the error functions, the generations will develop to have the minimum error function, or what is the same, each generation will be more suitable for the problem than the previous one.

The genetic algorithm used in this work is the one embedded in Matlab®, which allows a wide flexibility in the design of the algorithm at the same time it gives default values that ease the design process. Regarding the genetic operators, they are defined by default in the following way:

1. Reproduction is defined in this case by the number of individuals that are guaranteed to survive to the next generation, usually the best ones, and the number of individuals that will be part of the next generation that are produced by recombination. The former is defined by a number of individuals and the latter by a fraction between 0 and 1. These last entries are actually part of the selection process.

2. Mutation is defined by a random function, by default Gaussian with 0 mean, that will add a random number to each entry of the parents vectors. The standard deviation can be defined to select the magnitude of the effect of mutations in the evolution process.

3. Recombination or crossover is defined by a crossover function. By default, Matlab® randomly creates a binary vector of the length of the chromosome and selects the gen from one parent when the vector is 1 and from the other when the vector is 0.

4. Selection is defined by default by an uniform function that picks a subgroup of the calculated individuals by randomly selecting the first one and then, selecting the other by a constant distant defined by the chromosome.

Regarding constraints, they take the form of a vector where the elements are operations of inequality that must be accomplished by all individuals. In practice, Matlab® uses an algorithm that keeps a maximum number of individuals per generation that can violate the constraints. Obviously, these individuals are never selected for the next generation or recombination. Finally, by stating the generation size, the algorithm is ready to start.

Chapter 3

Radiative cooling designs

In this chapter, three different designs for radiative cooling are presented. The first one is a metasurface designed and manufactured in 2017 that takes advantage of advances in nanofabrication technologies. The second device is a near ideal perfect emitter for radiative cooling, which has a near maximum net cooling power. Nevertheless, its fabrication is actually difficult for current technologies. Lastly, a multilayered structure with the materials introduced in Chapter 2 is studied using the analytical methods of Section 2.5 and the optimization method of Section 2.6.

3.1 Metasurface

The structure presented in [13] is a metasurface that consists of two silicon islands of the same dimensions but oriented on different axes. Such islands are repeated periodically over the x and y axes, and are put on a silicon substrate. All the top surfaces are coated with a silver layer. The unit cell that represents the full structure and is going to be analyzed is depicted in Fig. 3.1.

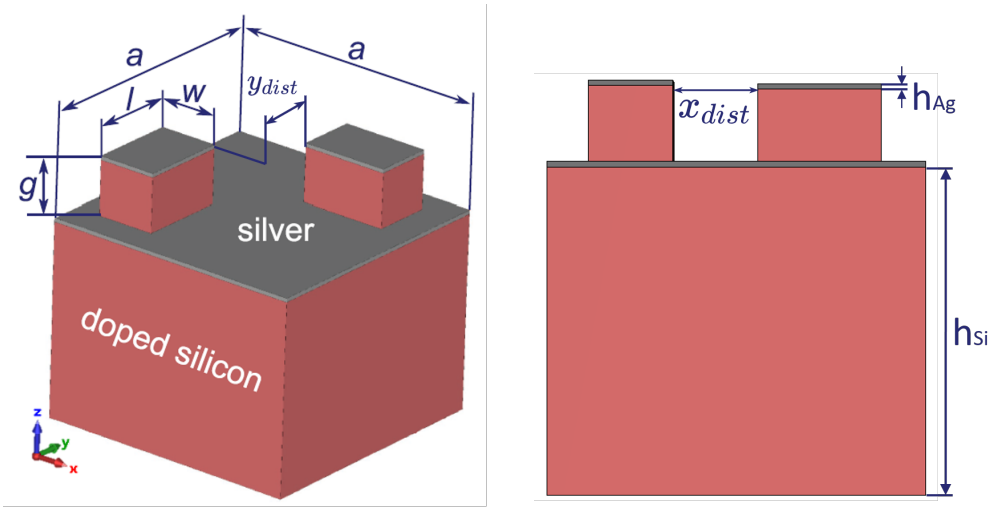

FIGURE 3.1: Metasurface presented in [13]: (a) unit cell in perspective and (b) side view of the unit cell

The proposed dimensions for the structure are, following Fig. 3.1: the periodicity length a = 6.9 μm, the islands height g = 1.5 μm, the length and the width of the islands, l = 2.3 μm and w = 1.55 μm. Then, the thickness of the silver layer h_{Ag} = 0.1 μm and the silicon substrate h_{Si} = 6 μm. Lastly, the distance between the islands in each axe will be x_{dist} = 1.55 μm and y_{dist} = 1.55 μm. While the silver layer is the one

introduced in Chapter 2, the silicon layer is doped with phosphorous and, therefore, is defined in the paper by a Drude model (Eq. 2.6) with the parameters of Table 3.1.

TABLE 3.1: Drude model of phosporous doped silicon of [13]

Epsilon infinite	Plasma frequency f_p	Collision frequency Γ
11.68	48.862 THz	8.806 THz

This permittivity model exhibits the following curve:

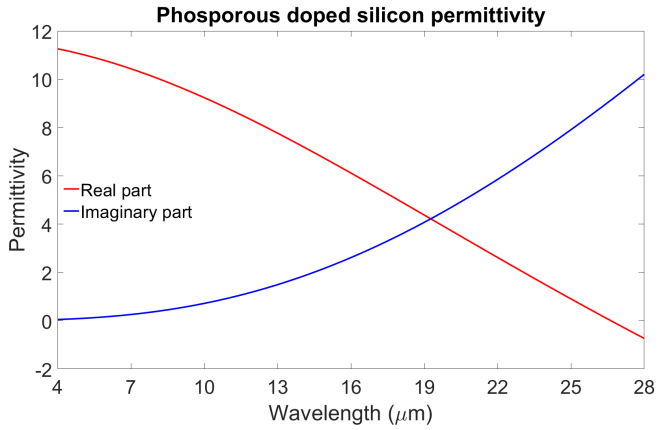

FIGURE 3.2: Phosporous doped silicon permittivity

This structure is simulated in CST by establishing periodic boundary conditions and Floquet ports in the mid infrared range: 4 μm - 26 μm. The obtained emissivity curve is depicted in Fig. 3.3.

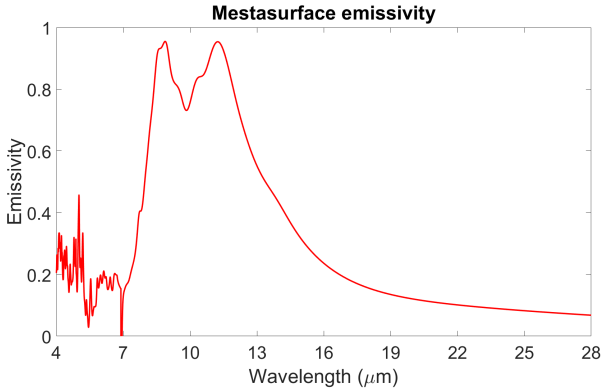

FIGURE 3.3: Simulated emissivity of the metasurface of [13]

It can be seen that the structure has a medium to high emissivity in the atmospheric window, from 8 μm to 13 μm. This wavelength response is not exactly the same as the one shown in [13], but is very similar to it. Considering that the structure is coated with a silver layer, it is expected to have a high solar reflection. In order to study the behaviour of the system and to enhance its performance, a parametric sweep of the parameters of the metasurface has been done. These are shown in Table 3.2 and their results presented in the following figures.

TABLE 3.2: Parametric sweep values for the metasurface introduced in [13]

Parameter	Interval	Step
a	5.9 μm - 7.9 μm	0.5 μm
g	0.5 μm - 2.5 μm	0.5 μm
l	1.3 μm - 2.8 μm	0.5 μm
w	0.55 μm - 2.55 μm	0.5 μm
$xdist$*	1.05 μm - 2.05 μm	0.5 μm
$ydist$*	1.05 μm - 2.05 μm	0.5 μm

*All combinations of these parameters have been considered

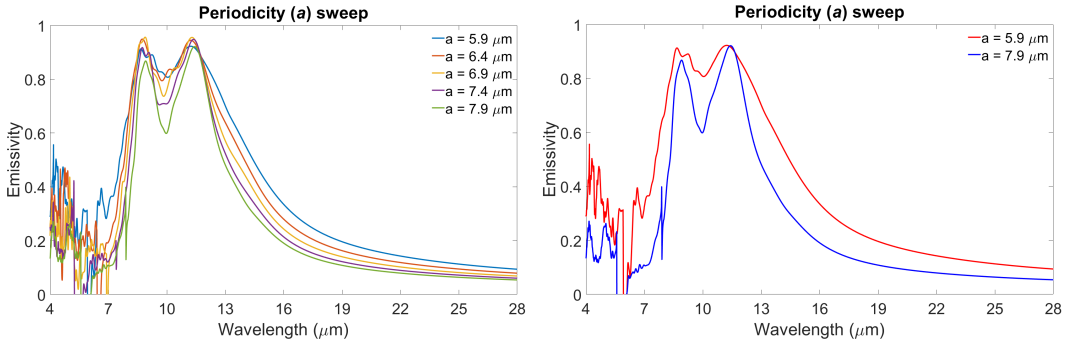

FIGURE 3.4: Parametric sweep of the metasurface periodicity, a: (a) all values and (b) maximum and minimum values

It can be seen in Fig. 3.4 that the unit cell size is actually important in the response of the metasurface. There is an inverse relationship between the the periodicity distance and the dip between the two peaks: the larger unit cell size the flatter the curve is in the emission bandwidth. Also, the emission increases in the lower wavelengths, which can have a negative effect for the solar reflection.

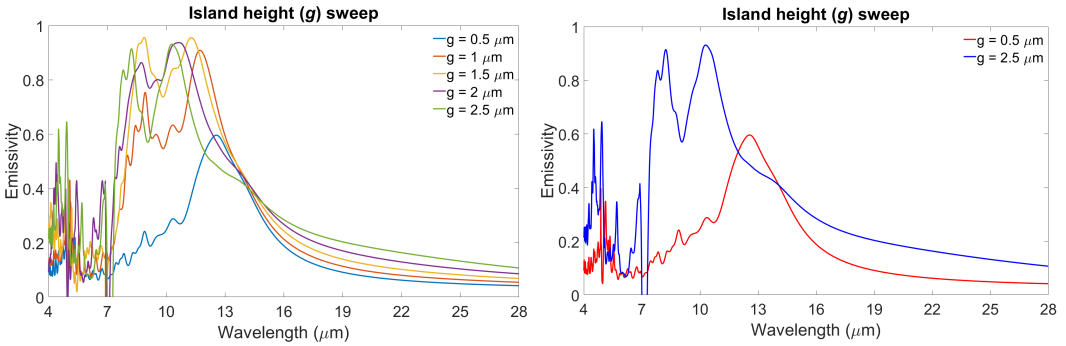

FIGURE 3.5: Parametric sweep of the metasurface island height, g: (a) all values and (b) maximum and minimum values

The island height appears to modulate the emission magnitude of the metasurface. If it is not sufficiently tall, the emission peak drops drastically, and the left side lobe disappears. Besides, it has its maximum emission spectra when g = 1.5 μm, which is nearly maintained for higher island height values. It also has a very weak

effect on the wavelength location of the emission peaks.

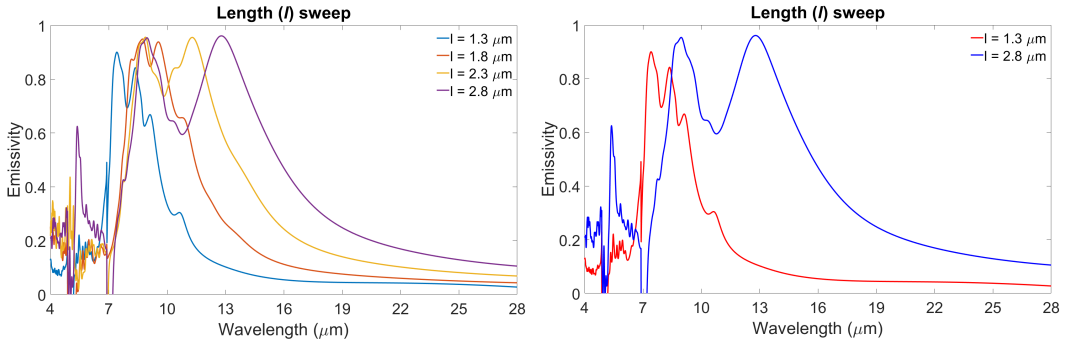

FIGURE 3.6: Parametric sweep of the metasurface island length, l: (a) all values and (b) maximum and minimum values

The island length has a direct relationship with the wavelength location of the emission band. Beside, it modifies the emissivity curve shape. This is because the two islands are very similar to a capacitor that changes with their size and, in a circuit, changing a capacity value leads to a substantial change in its frequency response. Also, when such length gets too small, say less than 1.8 μm, the right side emissivity lobe is suppressed. Regarding the lower and upper wavelengths, increasing the length leads to an increment in the emissivity.

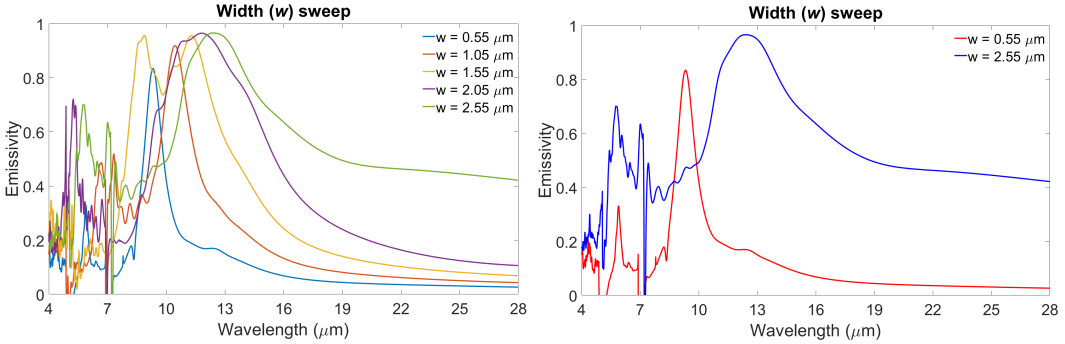

FIGURE 3.7: Parametric sweep of the metasurface island width, w: (a) all values and (b) maximum and minimum values

The island width also modifies drastically the emissivity curve. It has a similar relationship with the wavelength as the length, the wider the islands the higher the emission peak. But this relationship is weaker actually. The width also increases the overall emissivity of the device, which is not desirable out of the atmospheric window.

In Fig. 3.8, it can be seen that there is no significant differences if the distance between the islands is modified. This could mean that there is no electromagnetic interaction between them at a first glance.

Looking the overall tendency of the sweeps, it seems that the reference structure is already optimized because the emissivity in the atmospheric window and out of the window is always worse than the initial one. In order to achieve a better structure new optimization methods like the one presented in [15] will be necessary.

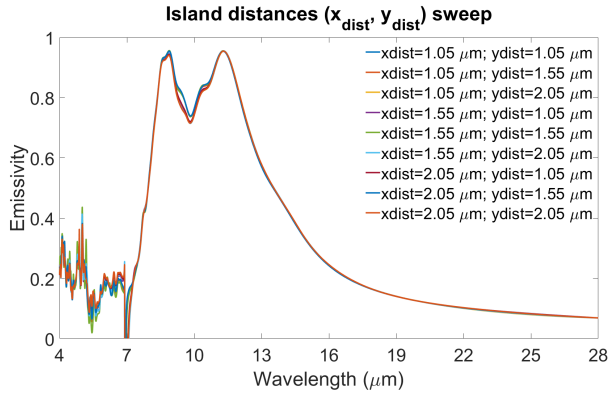

FIGURE 3.8: Island distances sweep

Regarding the net cooling power, the emission spectra for all elevation angles is required. Knowing the emissivity in the normal direction of the structure, the response in the other angles can be estimated by an inverse cosine angular dependence as the one of Eq. 1.3. This leads to the following angular emissivity:

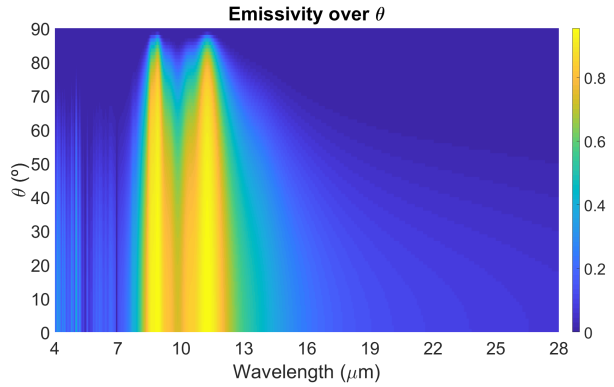

FIGURE 3.9: Angular emissivity of the metasurface

Considering an ambient temperature T_{atm} = 300 K (27ºC) and a device temperature of T = 294 K (21ºC), the emissivity of Fig. 3.9 leads to a night-time radiative cooling power of 62.92 W. This result differs from the one of the reference paper. The difference between them can be a cumulative effect of using a different extrapolation method for estimating the angle dependent emissivity, using different atmospheric models and the fact that the simulated emissivity is not exactly the same as the one found in the reference.

In order to know the behaviour of the net cooling power vs temperature, two temperature sweeps have been done with the spectra of Fig. 3.9. First, the net cooling power of the device is calculated for the temperature of the device T from -23ºC to 32ºC with a step of 5ºC, assuming an ambient temperature of 27ºC. Second, the net cooling power for an ambient temperature in a range from 7ºC to 57ºC with steps of 5ºC when the structure is at 21ºC. Both curves are plotted in Fig. 3.10.

It can be seen in the left curve that, for such conditions, the equilibrium temperature of the device is at -20ºC. This result indicates that, theoretically, the metasurface could achieve a temperature of -20ºC when the ambient is at 27ºC during the night.

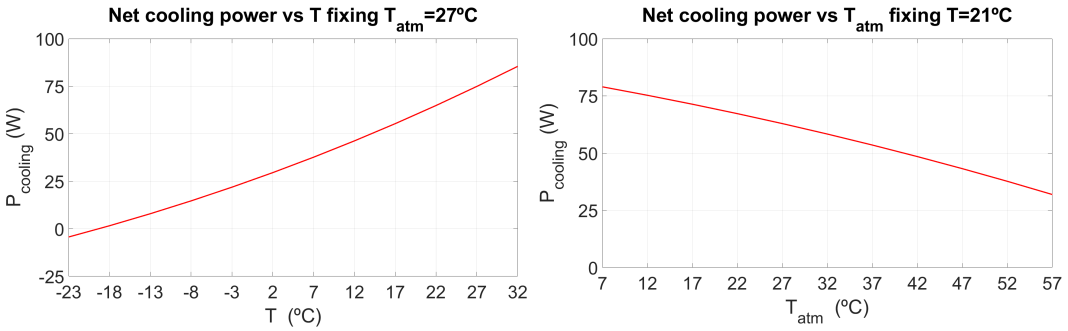

(a) (b)

FIGURE 3.10: Net cooling power of the metasurface over (a) temperature of device T fixing T_{atm}=27ºC, and (b) over ambient temperature T_{atm} fixing T=21ºC

Also, it is normal that the cooling power decreases with the temperature of the device because the black body radiation decreases. Moreover, at higher ambient temperatures, the cooling power also decreases due to absorption of more heat coming from the atmosphere.

3.2 Metastructure

The device presented in [11] is a pyramid shaped metamaterial with 19 layers. Each step of the pyramid is composed of two layers, one of silica and other of alumina, which have been characterized in Chapter 2. Such structure is located above a silver layer and is repeated periodically over the x and y axes. The metamaterial is illustrated in Fig. 3.11.

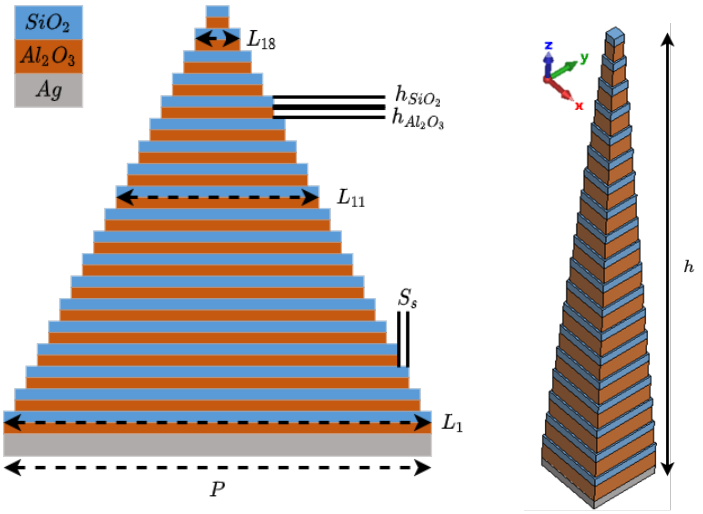

(a) (b)

FIGURE 3.11: Pyramidal metastructure of [11]: (a) side view of the unit cell and (b) unit cell in perspective

The proposed parameters of Fig. 3.11 are the height of the silica layer, h_{SiO_2} = 1 μm, the thickness of the alumina layer, $h_{Al_2O_3}$ = 2 μm, which makes a layer height of h_L = 3 μm, a formula for each layer length $L_n(\mu m) = 7.5 - (n-1) \times S_s$ with a

constant step size S_s = 0.35 μm and n as the layer number. Lastly, P = 7.5 μm is the period of the structure in the x and y axes and the height of the structure is h = 57 μm. The metamaterial is analyzed in CST and compared with GD-Calc, imposing periodic boundary conditions and Floquet ports in the mid infrared range: 4 μm - 26 μm. The obtained emissivity curve is depicted in Fig. 3.12.

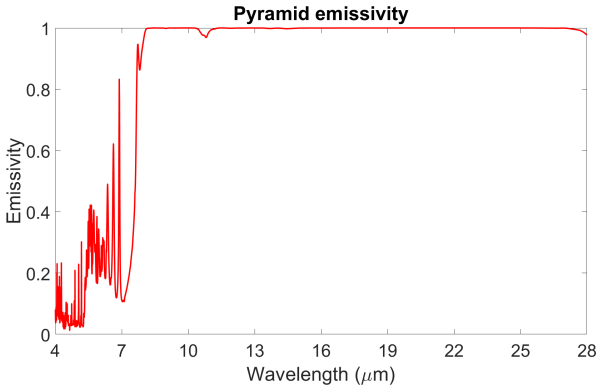

FIGURE 3.12: Simulated emissivity of the metastructure of [11]

In order to have a deeper knowledge of the behaviour of the pyramid, a few parametric sweeps have been done. First, the effect of the number of layers in the emissivity while maintaining its height is studied. In this case, the layer lengths are taken from the original structure, i.e., if there are 8 layers, the first layer will have a length equal to the base and the last one equal to L_{19}. Then, the intermediate lengths are selected to be equally spaced between them. Second, the number of layers giving a constant step change, thus changing the total height of the pyramid. Lastly, the effect of different step size between layers given a device composed of 8 layers is analyzed. All this is summarized in Table 3.3 and the results are shown in the following pictures.

TABLE 3.3: Parametric sweeps for the pyramidal metastructure of [11]

Parameter	Values	Notes
number of layers	2, 4, 6, 8	h = 57 μm
number of layers	2, 4, 6, 8	h_L = 3 μm
S_s	0.35 μm, 0.55 μm, 0.9 μm	8 layers
S_s	0.25 μm, 0.35 μm, 0.42 μm	16 layers

Looking at the results of Fig. 3.13, it seems that there is not a direct relationship between the number of layers and the response as long as the total height is maintained. Maybe the latter has a deeper effect in the emission spectrum of the device. Then, a sweep over the number of layers giving a constant layer height have been done. Its results are shown in Fig. 3.14.

Taking into account the plots depicted in Fig. 3.14, there is a direct relationship between the emission spectrum of the structure and the number of layers as long as the layer height is maintained. This can be the result of a less smooth permittivity change that a wave experiences when it tries to cross the pyramid. Following this idea, it is expected that some height is required with a fine step and a sharp geometry

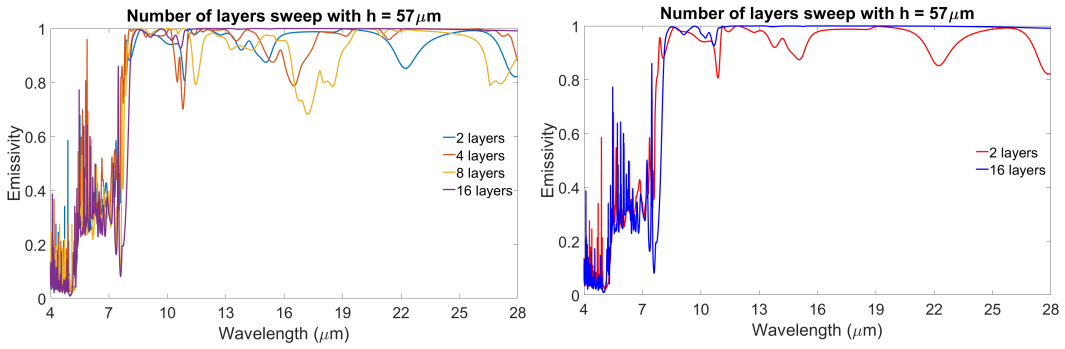

(a) (b)

FIGURE 3.13: Layer sweep with constant height: (a) all values and (b) maximum and minimum values

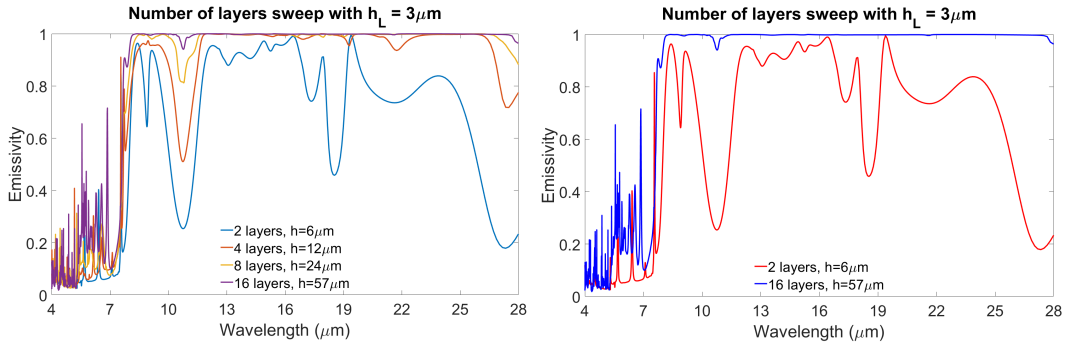

(a) (b)

FIGURE 3.14: Layer sweep with variable height: (a) all values and (b) maximum and minimum values

in order to smooth the permittivity change. Finally, the curves of the sweep over the step when there are 8 and 16 layers are shown in Fig. 3.15.

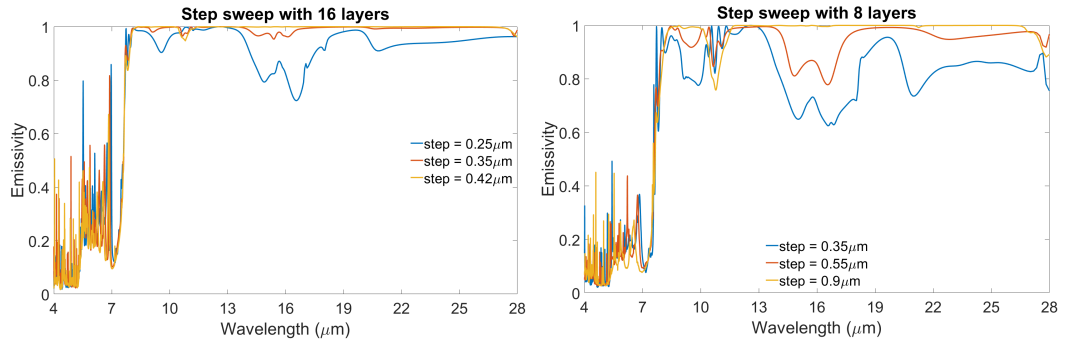

(a) (b)

FIGURE 3.15: Step sweep with: (a) 16 layers and (b) 8 layers

Looking at Fig. 3.15, it seems that the step is an important factor affecting the emissivity of the metastructure. It should be taken into account that the bigger step makes the sharper structure, while the others make a pyramid with a relatively big roof, which makes harder for the radiation to exit the structure due to the abrupt permittivity change between the device and free space.

In order to study the response in the solar spectrum (0.3 μm - 4 μm), GD-Calc has been used due to the limitations of CST for this application explained in Chapter 1. Before its use, the agreement between this simulator and CST has been analyzed. For that purpose, the response of a pyramid of 8 layers and a pyramid of 16 layers have been compared. Both results are shown in Fig. 3.16.

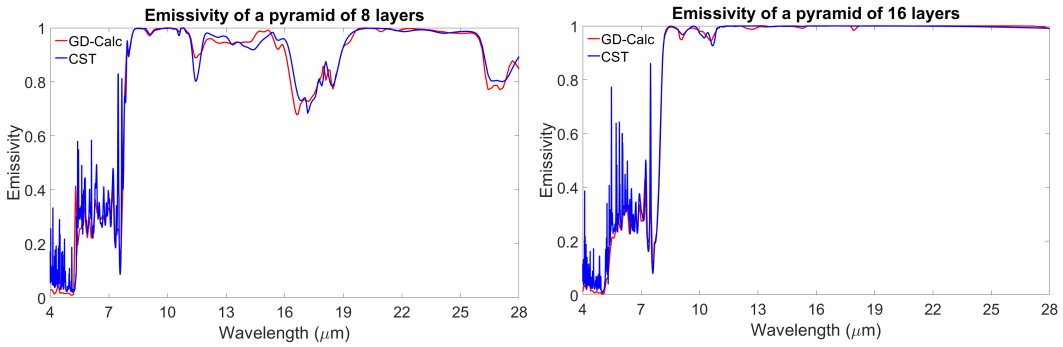

(a) (b)

FIGURE 3.16: Comparison between GD-Calc and CST for (a) an 8 layered pyramid and (b) 16 layered pyramid

It can be seen in Fig. 3.16 that the results of both simulators have a good agreement. Also, it should be considered that CST spends more than 4 and 2 hours to compute the pyramidal structures of 16 and 8 layers respectively while GD-Calc only needs less than 10 and 4 minutes. Also, GD-Calc does not need much more time to analyze the solar spectrum, in sharp contrast to CST, which actually cannot compute such bandwidth with the used hardware.

Then, the angular dependency has been studied thanks to the reduction of the computation time. The angles considered are: 0º, 15º, 30º, 45º, 60º, 75º and 89º for the reference structure. Using these angles, an interpolation can be done to compute the net cooling power with less error than the previous section. The emission spectrum at an angle of incidence of 90º is assumed to be zero. These curves are depicted in Fig. 3.17.

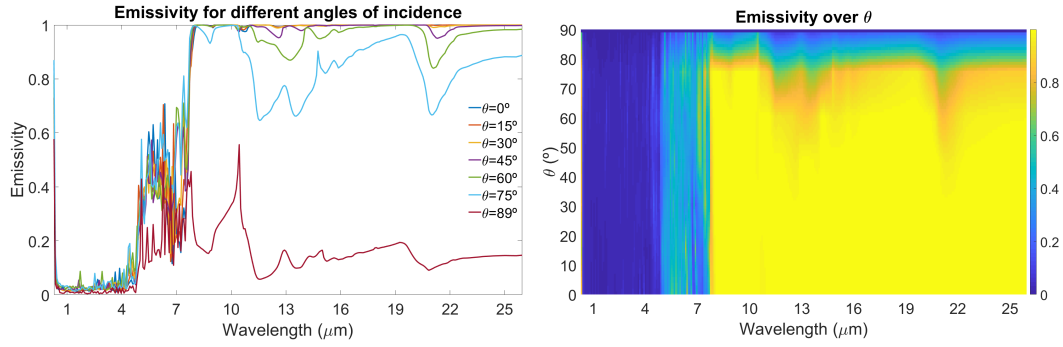

(a) (b)

FIGURE 3.17: Angle sweep of the metastructure: (a) simulated angles and (b) interpolation

As expected, the structure emissivity decays with the angle increment, but not as much as expected because the pyramid keeps a high emission spectrum at 75°. It also has a very high solar reflectivity, which makes the model suitable for day-time radiative cooling. Taking into account the theory of Chapter 1, this device will be very similar to an ideal radiator when the pyramid is at a high temperatures.

Taking into account only the interpolated emission angles, an ambient temperature of T_{atm} = 300 K (27ºC) and a temperature of a device of T = 294 K (21ºC), it can be calculated that the day-time net cooling power of the structure is 50 W. In order to know the behaviour of the net cooling power over temperature, two temperature sweeps have been done with the spectra of Fig. 3.17. The first one is of the temperature of the device, from 260 K (-13ºC) to 310 K (37ºC) and the second is of the ambient temperature, from 280 K (7ºC) to 330 K (57ºC). Both sweeps are done with a step of 5 K and depicted in Fig. 3.18.

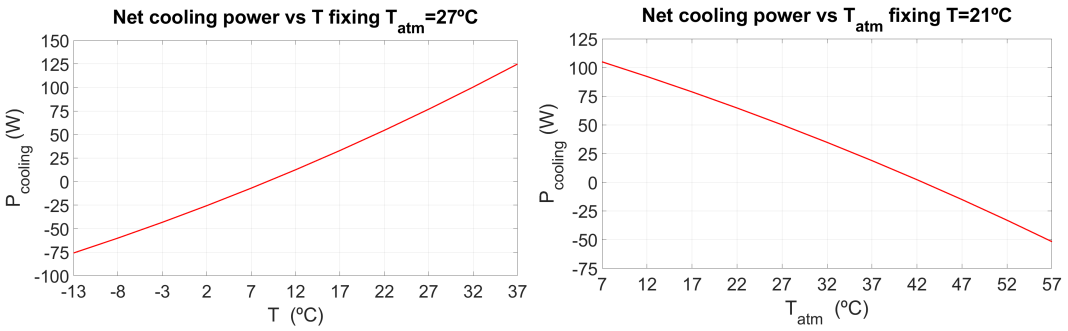

(a) (b)

FIGURE 3.18: Temperature sweep of the metastructure over (a) device temperature T fixing T_{atm}=27ºC, and (b) over ambient temperature T_{atm} fixing T=21ºC

Observing the curves, it can be seen that, under the supposed conditions, the thermal equilibrium of the structure under direct sunlight is of 10ºC. That means that in a day at 27ºC, such device will achieve a reduction of 17° under ambient temperature over time. Also, if both the device and ambient are at 27ºC, the net cooling power exceeds 75 W.

There are some differences between these results and the ones presented in the reference paper. This can be because the used atmospheric transmittance model and simulation tools are not the same.

3.3 Multi-layered structure

Taking into account the materials introduced in Chapter 2.2, a new multilayered structure with several degrees of freedom can be studied. Such structure will have a maximum of N layers of different materials that are theoretically infinite in their transverse plane and have some length in their normal direction. Each layer can be made of alumina, silicon nitride or silica and the system will be laying on an aluminium plate. A graphical illustration of the metastructure is depicted in Fig. 3.19.

This metamaterial raises one of the main current problems, which is that the optimization of a system with such an amount of degrees of freedom is in fact difficult. Therefore, the parametric sweeps used in previous sections have been replaced by

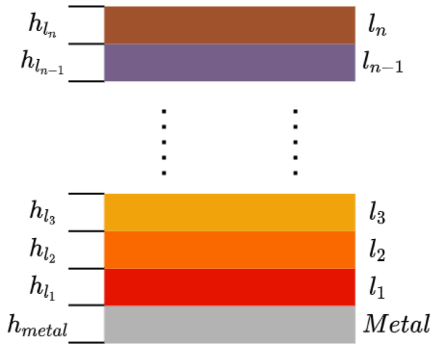

FIGURE 3.19: Multilayered structure

newer optimization techniques based on evolutionary algorithms, that have been introduced in Chapter 2.6. A first analysis has been done using a genetic algorithm, which is by default included in Matlab®.

In first place, the multilayered structure must be decomposed in a code that can be modified by the algorithm, the so called chromosome for each solution. The summary of the code of structure is presented in Table 3.4:

TABLE 3.4: First genetic algorithm code

Parameter	Values	Code
Number of layers	8	N/A
layer thickness (h_{l_n})	[0.1, 0.2, 0.4, 0.6, 0.8, 1, 1.5, 2] μm	[0-7]
layer material (l_n)	[Al_2O3, SiO_2, Si_3N_4]	[0, 1, 2]

In this case, the code is a vector of 16 integer numbers where the first 8 numbers establish the material of each layer starting from the top, and the least 8 numbers estate the layer thickness in the same order. The chromosome of an individual, i.e. [0, 1, 0, 1, 2, 1, 0, 1, 0, 6, 3, 6, 2, 5, 7, 1] will give the structure of layers [$l_8 = Al_2O_3$, $l_7 = SiO_2$, ... , $l_2 = SiO_2$, $l_1 = Al_2O_3$] with thicknesses of [h_{l_8} = 0.1 μm, h_{l_7} = 1.5 μm, ... , h_{l_2} = 2 μm, h_{l_1} = 0.2 μm] that will have a defined emissivity.

The sample space can be calculated by multiplying the possible materials for each layer and the possible thicknesses. Knowing that the first layer has no restriction in his material, thus, it has three possible materials, the sample space can be calculated as $3 \times 2^{N-1} \times 8^N = 6.4425 \times 10^9$, where 2 is the possible materials of each layer for not being able to repeat the previous layer material and 8 the possible values of thickness for each layer. N has been defined as the number of layers.

Then, the emissivity of each individual must be compared to some reference in order to give the objective to the evolutionary algorithm. In this case, the reference curve is an ideal radiator in the atmospheric window, from 7 μm to 13 μm, which has its emissivity curve depicted in Fig. 3.20. The metric in this case is the Mean Square Error(MSE) between the curve of the individual and the curve of the ideal radiator.

It should be considered that, due to time restrictions, the genetic algorithm is designed to optimize only the emission in the normal direction to the structure. In a deeper analysis, all emission angles should be considered in order to optimize the

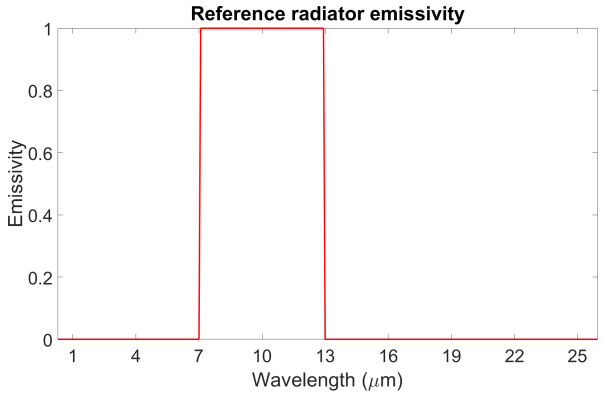

FIGURE 3.20: Reference radiator for the genetic algorithm

net cooling power. Moreover, the net cooling power is not taken by the algorithm because its computation for each individual would increment greatly the overall calculation time.

The genetic algorithm used has been configured to have a maximum number of generations of 1000, a maximum number of generations without improvement of 40, a population size of 100, a maximum computation time of 20 hours and the default mutation function is Gaussian. Also, it has the restriction of not being able to make two adjacent layers of the same material. It should be taken into account that, because the target is day-time radiative cooling, the error between the reference curve and the individual curve is weighted. So, not reducing the solar reflection means an error 10 times larger than not increasing the emission in the atmospheric window. These configurations of the genetic algorithm are summarized in Table 3.5 and its development in Fig. 3.21.

TABLE 3.5: First genetic algorithm configuration

Parameter	Values	Description
Max. Gen.	1000	Maximum number of generations
Pop. Size	100	Individuals per generation
Max. Stall Gen.	40	Maximum number of generations without improvement
Max. Time	20h	Maximum computation time
Error func.	MSE	Penalty function for individuals

The penalty value is the mean square error between the reference curve and the individual multiplied by 10 for the wavelength range below 4 μm, and multiplied by 1 for the wavelengths above. The best individual is defined by its code, introduced in Table 3.4. It can be seen that the algorithm only needed 143 generations, with 7707 individuals, to find a minimum for the penalty value, which can be a local minimum because this number represents only a 1.1963×10^{-4}% of the possible individuals. It can be seen that the best individual is not similar to the reference curve because its MSE is 0.138, thus, a nearly ideal radiator has not been found. The dimensions and emissivity of the best individual ever in this algorithm, the so called hall of fame (HOF), is shown in Fig. 3.22.

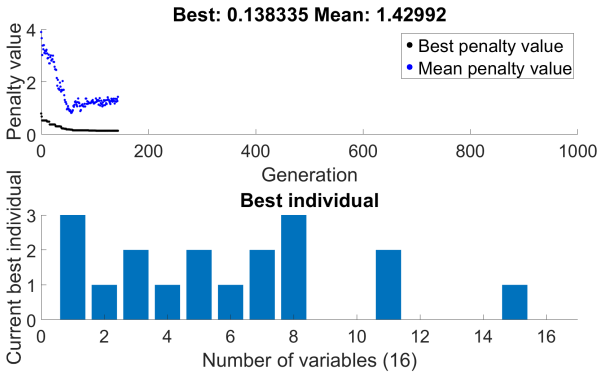

FIGURE 3.21: First genetic algorithm results

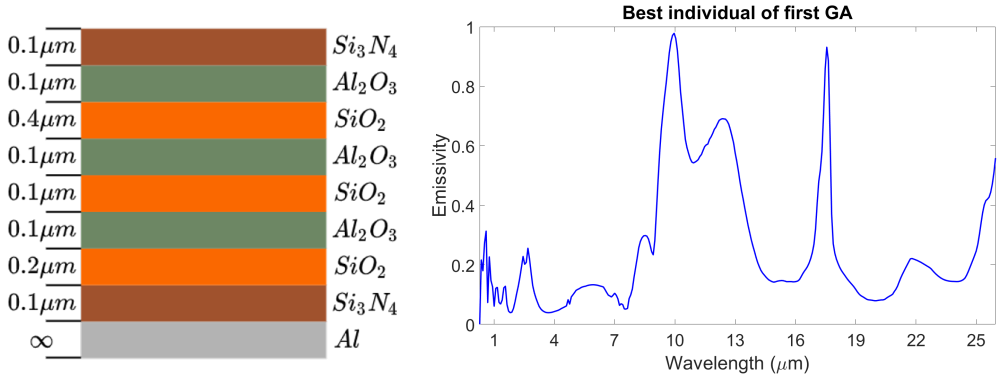

(a) (b)

FIGURE 3.22: Hall of fame of the first GA: (a) dimensions and (b) emissivity curve

The genetic algorithm has found a solution with a rather high selective emission in the atmospheric window. Nevertheless, the solar reflection is not enough to achieve day-time radiative cooling. Also, there is a clear preference for thin layers.

The fast convergence of the algorithm could mean that it has found a local minimum. An easy way to avoid it is to increase the mutation chance of the individuals or generations. The latter can be done by simply increasing the population size, which would increase the possibility for a generation to develop a new mutation. Also, the layer size tends to be lower than 0.5 μm, which can lead to a reduction in the sample space of a future optimization. This allows to increase the number of layers without increasing the sample space. Therefore, a new algorithm with a new code for individuals is designed, with both data summarized in Tables 3.6 and 3.7.

TABLE 3.6: Second genetic algorithm configuration

Parameter	Values	Description
Max. Gen.	1000	Maximum number of generations
Pop. Size	250	Individuals per generation
Max. Stall Gen.	250	Maximum number of generations without improvement
Max. Time	20h	Maximum computation time
Error func.	MSE	Penalty function for individuals

TABLE 3.7: Second genetic algorithm code

Parameter	Values	Code
Number of layers	10	N/A
layer thickness (h_{l_n})	[0.1, 0.2, 0.4, 0.6, 0.8] μm	[0-4]
layer material (l_n)	[Al_2O3, SiO_2, Si_3N_4]	[0, 1, 2]

In this case, the sample space is of 1.5×10^{10} and, in order to achieve a better solar reflection, the MSE for wavelengths below 4 μm is multiplied by a factor of 50. The development of this second genetic algorithm and its best individual are depicted in Fig. 3.23 and Fig. 3.24. In this case, the algorithm has again stopped because it has achieved the maximum number of generations without improvement at 423 generations and it has calculated the response of 187178 structures.

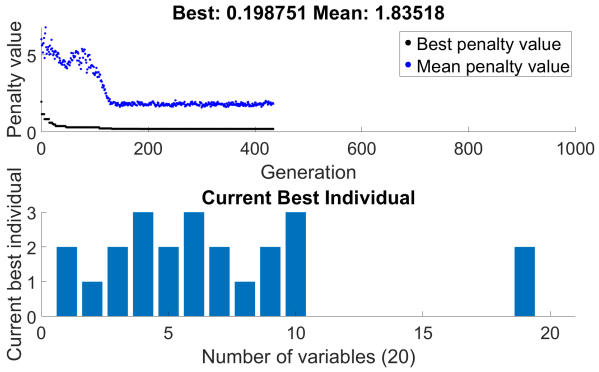

FIGURE 3.23: Second genetic algorithm results

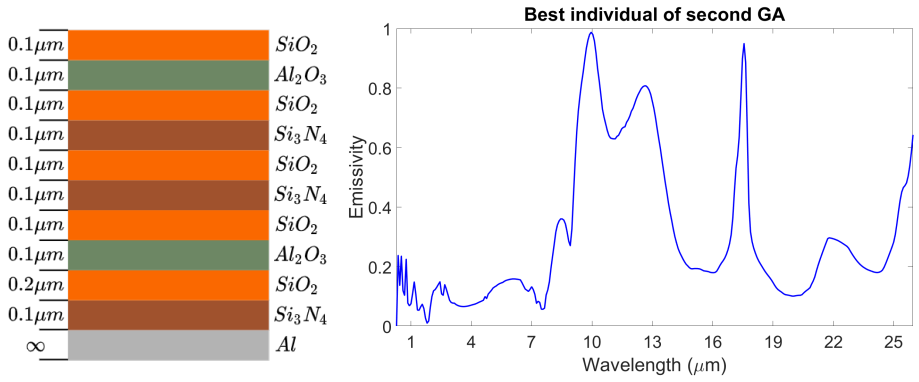

FIGURE 3.24: Hall of fame of the Second GA: (a) dimensions and (b) emissivity curve

Although in this second case the genetic algorithm have had more time to search for a better combination, it seems that little improvement has been achieved. In both cases a clear tendency to minimize the thicknesses of the layers can be seen and interestingly, the first four layers beginning from the metal plane in Figs. 3.22a and 3.24a, are equal in materials and thicknesses. In order to compare their performance, both structures have been analyzed varying the incidence angle θ from 0° to 89° in

steps of 1° and the results are depicted in Fig. 3.25.

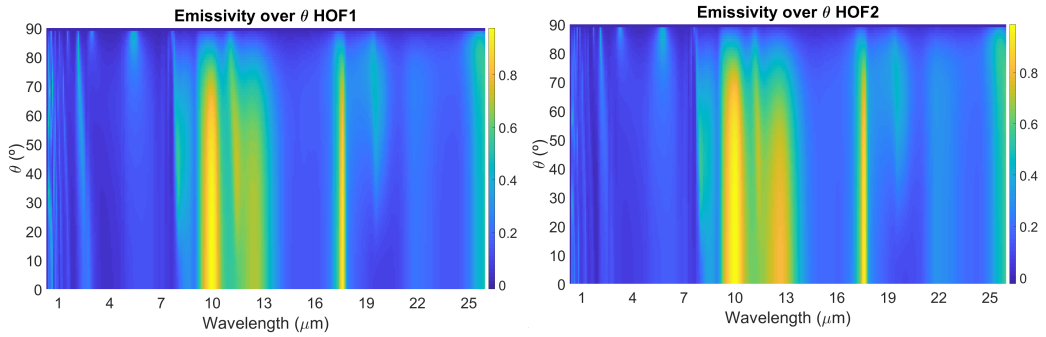

FIGURE 3.25: Thin film multilayered structures emissivities (a) first GA HOF and (b) second GA HOF

It can be seen that both devices are quite good selective emitters in the atmospheric window and that they have an overall emission relatively small. This can be beneficial for achieving a very low equilibrium temperature, but limits the maximum net cooling power when the device is at high temperatures. Also, the second structure has a higher emission in the atmospheric window

It can be seen that neither of them reflect enough the solar spectra to achieve daytime radiative cooling, and, therefore, the performance comparison between them is done under night-time conditions. Two temperature sweeps have been done, one for the device temperature and one for the ambient temperature. Both of them are depicted in Fig. 3.26:

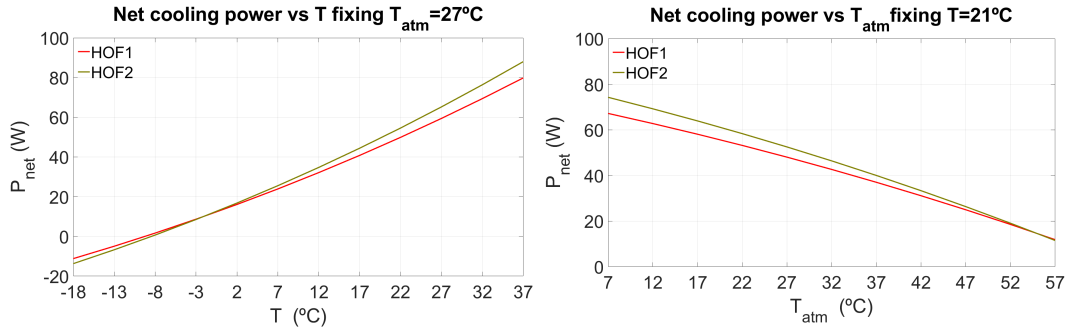

FIGURE 3.26: Temperature sweep of the multilayered structures over (a) device temperature T fixing T_{atm}=27ºC and (b) over ambient temperature T_{atm} fixing T=21ºC

Both structures achieve a positive net cooling power during the night. Also, due to being very selective emitters, the equilibrium temperature is at about -10ºC and they both keep quite well their net cooling power when the ambient is hot. Considering an ambient temperature of 27ºC and the device temperature of 21ºC, the first and second structures have achieved a night-time net cooling power of approximately 45 W and 50 W respectively. Therefore, the second optimization has lead to a slightly better device that also has a better solar reflection.

Chapter 4

Conclusions and future lines

Radiative cooling is an exploitable phenomenon for enhancing the current building energetic efficiency that need to be refrigerated, which implies a great reduction in energy expenses. Moreover, it has several applications in clothes, photovoltaic cells and vehicles which in combination could have an even greater impact on energy savings. This could have a very positive effect in global warming because it allows to balance the earth heat emission with the greenhouse effects and, therefore, radiative cooling should be considered as a tool against climate change.

In this master thesis, two analytical methods for calculating the reflectance and transmittance of thin film multilayered structures have been developed. They are based on transmission line theory and its analogy with plane waves. They both have been compared with GD-Calc®, which is a Matlab® semi analytic simulator for grating structures at optical frequencies that is based on the *Rigorous Coupled Wave Method* (RCWM). Also, another analytical method from [39] that is based on the combination of plane wave propagation with the law of Snell has been tested. All mathematical methods have given a negligible error in comparison to the simulator. Moreover, they have reduced the computation time by a factor greater than 250, which allowed to calculate all the emission angles to compute the net cooling power for the thin film multilayered structures.

Three main metamaterials for radiative cooling have been studied: a metasurface from [13], a pyramidal shaped metastructure from [11] and a thin film multilayered structure. The first two have been analyzed by parametric sweeps, giving the metasurface a night-time cooling power of 62.92 W/m^2 and the pyramid a day-time net cooling power of more than 75 W/m^2. The thin film multilayered structure have been designed with a genetic algorithm, which is an optimization method of the family of evolutionary algorithms. This leads to an automated design that has lead to a structure with a night-time net cooling power of nearly 50 W/m^2. The used atmospheric transmittance model assumes very harsh environmental conditions for radiative cooling, which is the main factor that explains the power difference between this work with the reference ones.

Although the designed thin film multilayered structure has not achieved sufficient solar reflection to operate during day, the optimization has relatively low solar absorption. Moreover, the night-time net cooling power could be drastically increased if the optimization is for such scenario. The mathematical models along with novel optimizations methods like evolutionary algorithms may solve the design problem in a near future for radiative cooling multilayered structures. This could lead to radiative cooling devices that are easy and fast to design and manufacture with potentially great cooling capacity.

On the counterpart, the mathematical models for more general metastructures that can lead to better radiative cooing devices are not developed and also, they are non trivial analytical problems. Moreover, the analytical models used in this work assume an ideal scenario with homogeneous media and perfect transitions between media. This will add some error between the simulations and the real device. Also, there is a need for developing accurate models for the thermal losses of the structures. Finally, the optimization algorithm has an underlying problem, which is that if different materials are about to be considered in optimization, the solution plane is non continuous. This means that an optimizer cannot guarantee its well behaviour if the curve to be optimized has abrupt variations with some parameters.

In the future, the optimizations should consider all incident angles and must be more customized for each problem. More materials should be included in the models in order to know to what extent the electromagnetic properties of a device can change using multilayered structures. Moreover, if the response is highly configurable, the ultimate step should be implementing a neural network that can make the inverse design. This means a machine that given a response, can design a multilayered structure that fulfills such behaviour. Regarding metamaterials, machine learning approaches can be also used to ease the design of such devices in case that the advances in fabrication methods allow their mass manufacturing for commercial applications in radiative cooling.

Regarding the atmospheric models, there is a lack of such models for different earth regions. Knowing the huge effect of them in the net cooling power, new models should be designed for the designing of radiative cooling devices of a given region or country. In the same line, the concept of time varying radiators, i.e., devices that can change their cooling power over time is not yet widely used. Those systems use phase changing materials to tune its electromagnetic response via temperature variation. This can have a huge impact by allowing devices that can cold in summer and heat in winter or simply by being controllable by an user.

Appendix A

Transmission line ended in a load

The general solution of a finite transmission line terminated in a load can be found in [41]. For the aim of this work, only the calculation of reflection and transmission coefficients is done. Consider the following set up:

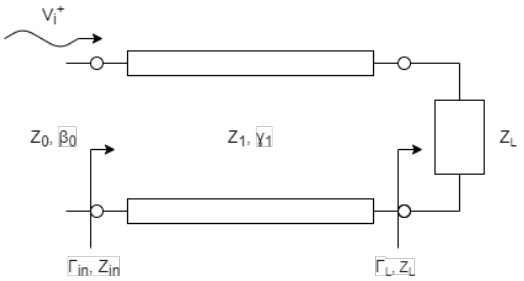

FIGURE A.1: Transmission line ended in a load

where V_i^+ is the progressive incident wave in the line, Z is the impedance of a line or element, β the propagation constant of an ideal line and γ the propagation constant of a lossy line. Z_{in} is the input impedance and Γ the reflection coefficient.

The reflection coefficient at the input of the transmission line can be calculated as:

$$\Gamma_{in} = \frac{Z_{in} - Z_1}{Z_{in} + Z_1} \tag{A.1}$$

where the input impedance Z_{in} can be obtained with the following formula:

$$Z_{in} = Z_1 \frac{Z_L + Z_1 tanh(\gamma_1 l_1)}{Z_1 + Z_L tanh(\gamma_1 l_1)} \tag{A.2}$$

where l_1 is the length of the line. For calculating the power given to the load, a voltage source must be considered, leading to the following scheme:

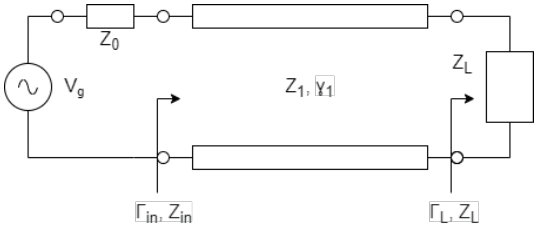

FIGURE A.2: Transmission line ended in a load with an input power

where V_g is the source voltage. In such scenario, the current at the input of the line I_{in} can be calculated as:

$$I_{in} = \frac{V_g}{Z_0 + Z_{in}} \tag{A.3}$$

Taking into account that the power is defined as $P = I^2R$, the power at the input of the transmission line is:

$$P_{in} = \frac{1}{2}|I_{in}|^2 Re(Z_{in}) \tag{A.4}$$

where Z_{in} is the complex input impedance of Eq. A.2. Finally, the power given at the load can be obtained as:

$$P_L = P_{in}e^{-2\alpha l_1}\frac{1-|\Gamma_L|^2}{1-|\Gamma_L|^2 e^{-4\alpha l_1}} \tag{A.5}$$

where α is the real part of the complex propagation constant γ of the transmission line. In order to know the transmission coefficient, the power at the input of the line must be calculated. The power at the input can be matched with the power of the generator, which by the Ohm law is:

$$P_g = \frac{|V_g|^2}{8Z_0} \tag{A.6}$$

where all terms have been previously defined. Finally, the transmission coefficient can be calculated by dividing the power delivered to the load by the input power:

$$T = \frac{P_L}{P_g} \tag{A.7}$$

Appendix B

ABCD and Scattering matrix

Microwave circuits can be represented in several ways, as explained in [42]. A typical manner is viewing such circuits as n-port networks, where the number of ports equals the number of inputs to the system. Between all the forms of describing such networks, the transmission matrix and scattering matrix general schemes are depicted in Fig. B.1.

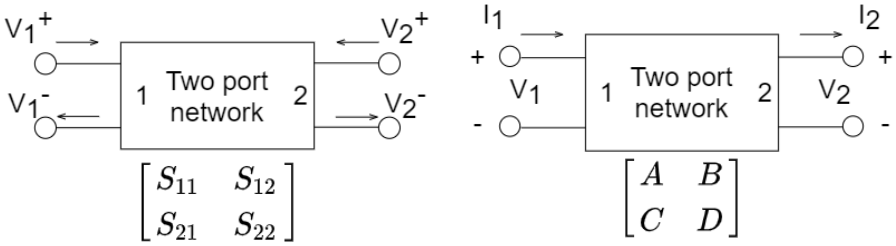

FIGURE B.1: (a) S matrix for a two port network and (b) ABCD matrix for a two port network

The scattering matrix, Fig. B.1a, is defined by the total progressive and regressive waves at each port, giving an easy way to calculate wave relationships. This will allow to estimate the reflection and transmission coefficients of a two port network. The elements of the matrix are defined as follows:

$$S_{11} = \frac{V_1^-}{V_1^+}|_{V_2^+=0} = \frac{reflected\ wave\ at\ port\ 1}{incident\ wave\ at\ port\ 1} \tag{B.1}$$

$$S_{12} = \frac{V_1^-}{V_2^+}|_{V_1^+=0} = \frac{transmitted\ wave\ at\ port\ 1}{incident\ wave\ at\ port\ 2} \tag{B.2}$$

$$S_{21} = \frac{V_2^-}{V_1^+}|_{V_2^+=0} = \frac{transmitted\ wave\ at\ port\ 2}{incident\ wave\ at\ port\ 1} \tag{B.3}$$

$$S_{22} = \frac{V_2^-}{V_2^+}|_{V_1^+=0} = \frac{reflected\ wave\ at\ port\ 2}{incident\ wave\ at\ port\ 2} \tag{B.4}$$

where $V_n^{\pm}$ is a voltage signal as described in equation 2.8. In Fig. B.1b is depicted the scheme of the ABCD matrix, also known as the transmission matrix. This matrix is defined by the total voltage and current at each port and gives a direct relationship between the input and the output. The definition is as follows:

$$\begin{bmatrix} V_1 \\ I_1 \end{bmatrix} = \begin{bmatrix} A & B \\ C & D \end{bmatrix} \begin{bmatrix} V_2 \\ I_2 \end{bmatrix} \tag{B.5}$$

This approach allows to compute multiple connected two port elements by multiplying their ABCD matrix. As shown in the following example:

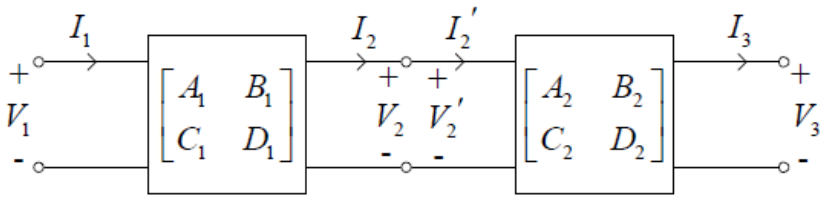

FIGURE B.2: ABCD matrix for two connected two port network

$$\begin{bmatrix} V_1 \\ I_1 \end{bmatrix} = \begin{bmatrix} A_1 & B_1 \\ C_1 & D_1 \end{bmatrix} \begin{bmatrix} A_2 & B_2 \\ C_2 & D_2 \end{bmatrix} \begin{bmatrix} V_3 \\ I_3 \end{bmatrix} \tag{B.6}$$

Also, it is well known from [43] that both matrix have direct relationship as follows :

$$S_{11} = \frac{AZ_{02} + B - CZ_{01}^{*}Z_{02} - DZ_{01}^{*}}{AZ_{02} + B + CZ_{01}Z_{02} + DZ_{01}} \tag{B.7}$$

$$S_{12} = \frac{2(AD - BC)(R_{01}R_{02})^{1/2}}{AZ_{02} + B + CZ_{01}Z_{02} + DZ_{01}} \tag{B.8}$$

$$S_{21} = \frac{2(R_{01}R_{02})^{1/2}}{AZ_{02} + B + CZ_{01}Z_{02} + DZ_{01}} \tag{B.9}$$

$$S_{22} = \frac{-AZ_{02}^{*} + B - CZ_{01}Z_{02}^{*} - DZ_{01}}{AZ_{02} + B + CZ_{01}Z_{02} + DZ_{01}} \tag{B.10}$$

Being Z_{01} and Z_{02} respectively the impedances of the input medium (at port 1) and the output medium (at port 2) with real parts R_{01} and R_{02}. Also, the * symbol indicates the complex conjugate of a number. This equations consider two mediums with different and complex impedance.

Therefore, the combination of these two representations allows to concatenate microwave circuits and calculate the total characteristics of the combination.

Bibliography

[1] C. T. S. E. of Astronomy, *Kirchhoff law of thermal radiation*, https://en.wikipedia.org/wiki/Kirchhoff%27s_law_of_thermal_radiation, Accessed: 16-04-2021.

[2] B. TL, L. AS, I. FP, and D. DP, *Fundamentals of heat and mass transfer*. John Wiley & Sons, 2011, ch. 4.

[3] K. Mansouri, "Passive radiative cooling using metasurfaces," M.S. thesis, Public University of Navarre, Jun. 2019.

[4] B. Zhao, M. Hu, X. Ao, N. Chen, and G. Pei, "Radiative cooling: A review of fundamentals, materials, applications, and prospects," *Applied Energy*, vol. 236, pp. 489–513, 2019, ISSN: 0306-2619. DOI: https://doi.org/10.1016/j.apenergy.2018.12.018.

[5] R. Family and M. P. Mengüç, "Materials for radiative cooling: A review," *Procedia Environmental Sciences*, vol. 38, pp. 752–759, 2017, Sustainable synergies from Buildings to the Urban Scale, ISSN: 1878-0296. DOI: https://doi.org/10.1016/j.proenv.2017.03.158.

[6] NREL, *Solar irradiance spectra*, https://www.nrel.gov/grid/solar-resource/spectra-am1.5.html, Accessed: 14-04-2021, 2000.

[7] Gemini Observatory, *Atmospheric transmittance spectra*, https://www.gemini.edu/sciops/telescopes-and-sites/observing-condition-constraints/ir-transmission-spectra, Accessed: 14-04-2021.

[8] AIN - Sistemas Inteligentes, UPNA - Instituto Smart Cities, *Pc005-006 aevometa*, https://www.ain.es/archivo-proyectos/aevometa/, Convocatoria de 2020 de ayudas a Centros tecnológicos y Organismos de investigación para la realización de proyectos de I+D colaborativos.

[9] M. Hu, G. Pei, Q. Wang, J. Li, Y. Wang, and J. Ji, "Field test and preliminary analysis of a combined diurnal solar heating and nocturnal radiative cooling system," *Applied Energy*, vol. 179, pp. 899–908, 2016, ISSN: 0306-2619. DOI: https://doi.org/10.1016/j.apenergy.2016.07.066.

[10] A. Harrison and M. Walton, "Radiative cooling of tio2 white paint," *Solar Energy*, vol. 20, no. 2, pp. 185–188, 1978, ISSN: 0038-092X. DOI: https://doi.org/10.1016/0038-092X(78)90195-0.

[11] D. Wu, C. Liu, Z. Xu, Y. Liu, Z. Yu, L. Yu, L. Chen, R. Li, R. Ma, and H. Ye, "The design of ultra-broadband selective near-perfect absorber based on photonic structures to achieve near-ideal daytime radiative cooling," *Materials & Design*, vol. 139, pp. 104–111, 2018, ISSN: 0264-1275. DOI: https://doi.org/10.1016/j.matdes.2017.10.077.

[12] E. Rephaeli, A. Raman, and S. Fan, "Ultrabroadband photonic structures to achieve high-performance daytime radiative cooling," *Nano Letters*, vol. 13, no. 4, pp. 1457–1461, 2013, PMID: 23461597. DOI: 10.1021/nl4004283.

[13] C. Zou, G. Ren, M. M. Hossain, S. Nirantar, W. Withayachumnankul, T. Ahmed, M. Bhaskaran, S. Sriram, M. Gu, and C. Fumeaux, "Metal-loaded dielectric resonator metasurfaces for radiative cooling," *Advanced Optical Materials*, vol. 5, no. 20, p. 1 700 460, 2017. DOI: https://doi.org/10.1002/adom.201700460.

[14] M. M. Hossain, B. Jia, and M. Gu, "A metamaterial emitter for highly efficient radiative cooling," *Advanced Optical Materials*, vol. 3, no. 8, pp. 1047–1051, 2015. DOI: https://doi.org/10.1002/adom.201500119.

[15] R. S. Hegde, "Deep learning: A new tool for photonic nanostructure design," *Nanoscale Adv.*, vol. 2, pp. 1007–1023, 3 2020. DOI: 10.1039/C9NA00656G.

[16] C. Zhen, Z. Linxiao, R. Aaswath, and F. Shanhui, "Radiative cooling to deep sub-freezing temperatures through a 24-h day–night cycle," *Nature Communications*, vol. 7, 2016, ISSN: 2041-1723. DOI: https://doi.org/10.1038/ncomms13729.

[17] B. Zhao, M. Hu, X. Ao, and G. Pei, "Performance analysis of enhanced radiative cooling of solar cells based on a commercial silicon photovoltaic module," *Solar Energy*, vol. 176, pp. 248–255, 2018, ISSN: 0038-092X. DOI: https://doi.org/10.1016/j.solener.2018.10.043.

[18] Y. Zhai, Y. Ma, S. N. David, D. Zhao, R. Lou, G. Tan, R. Yang, and X. Yin, "Scalable-manufactured randomized glass-polymer hybrid metamaterial for daytime radiative cooling," *Science*, vol. 355, no. 6329, pp. 1062–1066, 2017, ISSN: 0036-8075. DOI: 10.1126/science.aai7899.

[19] J. K. Tong, X. Huang, S. V. Boriskina, J. Loomis, Y. Xu, and G. Chen, "Infrared-transparent visible-opaque fabrics for wearable personal thermal management," *ACS Photonics*, vol. 2, no. 6, pp. 769–778, 2015. DOI: 10.1021/acsphotonics.5b00140.

[20] T. Li, Y. Zhai, S. He, W. Gan, Z. Wei, M. Heidarinejad, D. Dalgo, R. Mi, X. Zhao, J. Song, J. Dai, C. Chen, A. Aili, A. Vellore, A. Martini, R. Yang, J. Srebric, X. Yin, and L. Hu, "A radiative cooling structural material," *Science*, vol. 364, no. 6442, pp. 760–763, 2019, ISSN: 0036-8075. DOI: 10.1126/science.aau9101.

[21] W. Wang, N. Fernandez, S. Katipamula, and K. Alvine, "Performance assessment of a photonic radiative cooling system for office buildings," *Renewable Energy*, vol. 118, pp. 265–277, 2018, ISSN: 0960-1481. DOI: https://doi.org/10.1016/j.renene.2017.10.062.

[22] X. Li, B. Sun, C. Sui, A. Nandi, H. Fang, Y. Peng, G. Tan, and P.-C. Hsu, "Integration of daytime radiative cooling and solar heating for year-round energy saving in buildings," *Nature Communications*, vol. 11, Nov. 2020. DOI: 10.1038/s41467-020-19790-x.

[23] E. D. Palik and G. Ghosh, *Handbook of optical constants of solids*. John Wiley & Sons, 1997.

[24] Mikhail Polyanskiy, *Refractive index*, https://refractiveindex.info/, Accessed: 06-05-2021, 2008.

[25] S. Paradis and J.-B. a. Keptsu, "Characterization and optimization of sio2 and si3n4 thin films for a smart uncooled ir sensor," M.S. thesis, Defence Research and Development Canada, Feb. 2013, ch. 3, pp. 11–15.

[26] J. Yang, X. Gao, Y. Wu, T. Zhang, H. Zeng, and X. Li, "Nanoporous silica microspheres–ploymethylpentene (tpx) hybrid films toward effective daytime radiative cooling," *Solar Energy Materials and Solar Cells*, vol. 206, p. 110 301, 2020, ISSN: 0927-0248. DOI: https://doi.org/10.1016/j.solmat.2019.110301.

[27] B. Zhao, M. Hu, X. Ao, and G. Pei, "Performance analysis of enhanced radiative cooling of solar cells based on a commercial silicon photovoltaic module," *Solar Energy*, vol. 176, pp. 248–255, 2018, ISSN: 0038-092X. DOI: https://doi.org/10.1016/j.solener.2018.10.043.

[28] M. M. Hossain, B. Jia, and M. Gu, "A metamaterial emitter for highly efficient radiative cooling," *Advanced Optical Materials*, vol. 3, no. 8, pp. 1047–1051, 2015. DOI: https://doi.org/10.1002/adom.201500119.

[29] W. Yu, Y. Lu, X. Chen, H. Xu, J. Shao, X. Chen, Y. Sun, J. Hao, and N. Dai, "Large-area, broadband, wide-angle plasmonic metasurface absorber for mid-wavelength infrared atmospheric transparency window," *Advanced Optical Materials*, vol. 7, no. 20, p. 1 900 841, 2019. DOI: https://doi.org/10.1002/adom.201900841.

[30] K. Sun, C. A. Riedel, Y. Wang, A. Urbani, M. Simeoni, S. Mengali, M. Zalkovskij, B. Bilenberg, C. H. de Groot, and O. L. Muskens, "Metasurface optical solar reflectors using azo transparent conducting oxides for radiative cooling of spacecraft," *ACS Photonics*, vol. 5, no. 2, pp. 495–501, 2018. DOI: 10.1021/acsphotonics.7b00991.

[31] J. Zhang, R. Wei, M. ElKabbash, E. M. Campbell, and C. Guo, "Thin-film perfect infrared absorbers over single- and dual-band atmospheric windows," *Opt. Lett.*, vol. 45, no. 10, pp. 2800–2803, May 2020. DOI: 10.1364/OL.392651.

[32] R. A., A. M., and L. e. a. Zhu, "Passive radiative cooling below ambient air temperature under direct sunlight," *Nature*, no. 515, 540–544, 2014. DOI: https://doi.org/10.1038/nature13883.

[33] Y. Qu, L. Cai, H. Luo, J. Lu, M. Qiu, and Q. Li, "Tunable dual-band thermal emitter consisting of single-sized phase-changing gst nanodisks," *Opt. Express*, vol. 26, no. 4, pp. 4279–4287, Feb. 2018. DOI: 10.1364/OE.26.004279.

[34] W.-W. Zhang, H. Qi, A.-T. Sun, Y.-T. Ren, and J.-W. Shi, "Periodic trapezoidal vo2-ge multilayer absorber for dynamic radiative cooling," *Opt. Express*, vol. 28, no. 14, pp. 20 609–20 623, Jul. 2020. DOI: 10.1364/OE.396171.

[35] M. Ono, K. Chen, W. Li, and S. Fan, "Self-adaptive radiative cooling based on phase change materials," *Opt. Express*, vol. 26, no. 18, A777–A787, Sep. 2018. DOI: 10.1364/OE.26.00A777.

[36] J.-W. Cho, T.-I. Lee, D.-S. Kim, K.-H. Park, Y.-S. Kim, and S.-K. Kim, "Visible to near-infrared thermal radiation from nanostructured tungsten anntennas," *Journal of Optics*, vol. 20, no. 9, 09LT01, Aug. 2018. DOI: 10.1088/2040-8986/aad708.

[37] Kenneth C. Johnson (KJ Innovation, *Grating diffraction calculator (gd-calc ®)*, https://codeocean.com/capsule/8614002/tree/v3, Accessed: 2021-05-13, 2019.

[38] Kenneth C. Johnson, *Kj innovation*, https://kjinnovation.com/, Accessed: 2021-05-13, 2019.

[39] Z. M. Zhang and C. J. Fu, "Unusual photon tunneling in the presence of a layer with a negative refractive index," *Applied Physics Letters*, vol. 80, no. 6, pp. 1097–1099, 2002. DOI: 10.1063/1.1448172.

[40] S. Ramo, J. R. Whinnery, and T. V. Duzer, *Fields and waves in communication electronics*. Wiley, 2013, ch. 5,11.

[41] D. M. Pozar, *Microwave Engineering*. Wiley, 2013, ch. 3,4.

[42] R. E. Collin, *Foundations for Microwave Engineering*. Wiley-Interscience, 1992, ch. 4.

[43] D. A. Frickey, "Conversions between s, z, y, h, abcd, and t parameters which are valid for complex source and load impedances," *IEEE transactions on microwave theory ans techniques*, vol. 42, no. 2, pp. 205–211, Feb. 1994. [Online]. Available: https://ieeexplore.ieee.org/document/275248.